GeoScienceWorld
Lithosphere
Volume 2024, Number Special 15, Article ID lithosphere_2024_183, 21 pages
https://doi.org/10.2113/2024/lithosphere_2024_183

Lithosphere

Research Article

Unravelling the Sequence and Timing of Fault-Related Deformation in Superimposed Rift Basins, Inner Moray Firth, NE Scotland

Alexandra Tamas[1], **Robert E. Holdsworth**[2,3], **Dan M. Tamas**[1], **Edward D. Dempsey**[4], **Kit Hardman**[4], **Anna Bird**[4], **John R. Underhill**[5], **Dave McCarthy**[6], **Ken J. W. McCaffrey**[2,3] and **David Selby**[2]

[1]*Department of Geology, Babes-Bolyai University, Cluj-Napoca, 400084, Romania*
[2]*Department of Earth Sciences, Durham University, Durham, DH1 3LE, United Kingdom*
[3]*Geospatial Research Ltd, Durham, DH1 5HL, United Kingdom*
[4]*Department of Geology, Hull University, Hull, HU6 7RX, United Kingdom*
[5]*School of Geosciences, University of Aberdeen, Aberdeen, AB24 3FX, United Kingdom*
[6]*Decarbonisation and Resource Management, British Geological Survey, Edinburgh, EH28 8AA, United Kingdom*

Correspondence should be addressed to Dan M. Tamas; danmircea.tamas@ubbcluj.ro

Received 29 June 2024; Accepted 25 February 2025; Published 21 April 2025

Academic Editor: Steve Banham

Devonian rocks of the Palaeozoic Orcadian Basin are well exposed along the northern flanks of the younger Mesozoic to Cenozoic Inner Moray Firth Basin in Scotland. These rocks preserve a succession of structures related to superimposed rifting and inversion events spanning nearly 400 Myrs. We combine new detailed field observations augmented by drone photography and the creation of 3D digital outcrops, coupled with U-Pb geochronology of syn-faulting calcite-mineralized veins to better constrain the absolute timing of fault movements and decipher the kinematic history of basin opening and inversion.Using this approach, we were able to isolate characteristic structures, fault kinematics, fault rock development and associated mineralization types related to five regional deformation events: (1) Devonian transtensional rifting associated to sinistral Great Glan Fault movements leading to the development of the Orcadian Basin; (2) Late Carboniferous inversion related to dextral Great Glen Fault reactivation; (3) minor N-S, possibly Permian calcite veins; (4) Late Jurassic–Early Cretaceous rifting related to the development of the IMFB; and finally, (5) Cenozoic uplift, reactivation, and local inversion. Our study demonstrates the utility of microstructurally constrained U-Pb geochronology of fault-related calcite mineralization. Applied elsewhere, our methodology has the potential to give consistent and regionally significant new insights into the nature and timing of superimposed rift-related deformation processes worldwide.

1. INTRODUCTION

Geological faults are one of the main manifestations of upper crustal deformation on planet Earth. They also substantially control the location and geometry of sedimentary basins at the surface, the evolution of accommodation space and internal sediment distribution pathways, and the channeling of subsurface to near-surface fluid flow (e.g. [1, 2]). These same faults are commonly reactivated during later episodes of rifting or inversion leading to complex, localized deformation zones (e.g. [3–5]), which can further impact on the development of subsurface resources and applications (e.g. minerals, hydrocarbons, geothermal, energy, and CO_2 storage). On a more regional scale, many continental basins are superimposed partially or completely over the sites of older, preexisting basins, for example Colorado Basin [6], East African Rift [7, 8], the Gulf of Aden [9], the North Atlantic margins [10–12], and more local to this study, the North Sea Rift (e.g. [12]) and the West Orkney Basin [13] (Figure 1).

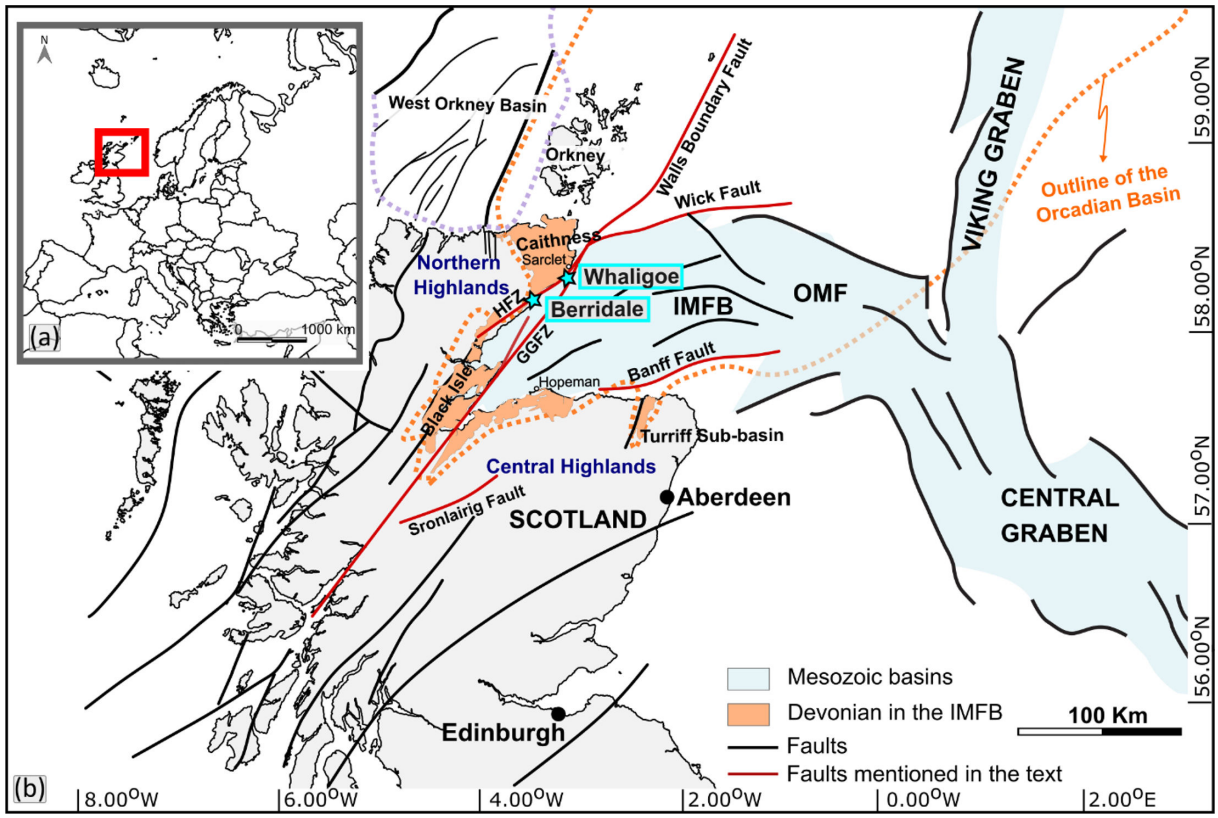

FIGURE 1: Location of the study area (a) regional administrative boundaries [based on GISCO—Eurostat (European Commission) data, © EuroGeographics © UN-FAO © Turkstat] showing the location of (b) generalized tectonic map of Scotland and the northern North Sea region showing the main Mesozoic rift systems (blue shading; adapted after [56]). IMFB, Inner Moray Firth Basin; OMF, Outer Moray Firth Basin. GGFZ, Great Glen Fault Zone, HFZ, Helmsdale Fault Zone. Outline of the Orcadian Basin marked in dotted orange line (after [27]) and outline of the West Orkney Basin is marked in dotted purple line (after [57]). The studied exposures are indicated by the blue star.

In all of these settings, the age of faulting and role of inherited structures is commonly difficult to constrain due to either the limited resolution (or absence) of seismic reflection data in offshore regions, while onshore areas may be limited by restricted surface exposure and lack of evidence to constrain the absolute age of fault movements. One potentially useful approach onshore is to focus on well-exposed coastal outcrops where structures imaged offshore can be traced directly or recognized indirectly based on orientation. In many cases, individual faulting or reactivation episodes will be associated with specific syn-tectonic mineral fills—such as calcite or base metal sulphides—which can then be dated using radiometric methods (e.g. U-Pb calcite and Re-Os sulfide, respectively) to constrain the age of specific faulting episodes (e.g. following the approaches outlined by [14, 15]).

The Inner Moray Firth Basin (Figure 1) is widely regarded as a classic example of a Mesozoic-Cenozoic intracontinental rift zone (e.g. [16]). It is also a superimposed rift that is located above part of an older, larger Palaeozoic feature, the Devonian Orcadian Basin (Figure 1; [17, 18]). U-Pb calcite and Re-Os sulfide geochronology has recently been used in these basins to explore the ages and histories of Palaeozoic and Mesozoic faulting and reactivation (e.g. [14, 19–22]). In this article, we further extend this approach using new field observations and microstructural observations to constrain U-Pb dating of calcite mineralization associated with deformation of Devonian strata located immediately north of the Helmsdale Fault on the northern flank of the Inner Moray Firth Basin. Taken together with the recent findings in adjacent areas, these results allow the recognition of five phases of faulting and reactivation from the Palaeozoic (Devonian, Late Carboniferous, and Permian), Mesozoic (Late Jurassic), and Cenozoic to be recognized along the northern margin of the Inner Moray Firth Basin. These findings further illustrate the value of U-Pb calcite dating to better constrain the timing of complex regional fault movements and reactivation in superimposed rift basin systems (e.g. [23]).

2. GEOLOGICAL OVERVIEW

The Orcadian Basin rests unconformably on Precambrian Moine and Lewisian metamorphic basement and early Devonian Helmsdale granite and is covered by younger Permian to Cretaceous sedimentary units of the Inner Moray Firth Basin (Figure 2). Devonian strata related to the Orcadian Basin are well exposed in onshore cliffs located along the north-western margin of the younger, offshore Mesozoic-Cenozoic Inner Moray Firth Basin, in eastern

(Whaligoe) and southern (Berridale) Caithness (Figure 1). The strata comprise mainly Middle Devonian, generally syn-rift alluvial, fluvial, lacustrine to locally marine sequences which unconformably overlie locally preserved Lower Devonian syn-rift alluvial and fluvial-lacustrine deposits located mainly close to the marginal parts of the Orcadian Basin (e.g. [18, 24, 25]). These are overlain locally in northern Caithness and Orkney by Upper Devonian postrift fluvial and marginal aeolian sedimentary rocks [18].

The Inner Moray Firth Basin margin here is strongly controlled by the Helmsdale and Great Glen faults (Figure 1), which together with the Banff Fault and Wick Fault form the main bounding structures of the basin ([21, 22] and references therein).

2.1. Palaeozoic Events

The Devonian-Carboniferous Orcadian Basin extends both onshore and offshore in the Inner Moray Firth Basin, Caithness, and Orkney regions (Figure 1; [17, 18]). It is part of a much larger system of Devonian basins that ranges northwards into Shetland, western Norway and eastern Greenland [26–29].

The Orcadian Basin formed in a transtensional setting and was associated with sinistral displacements along the Great Glen Fault Zone during the early- to mid-Devonian which led to the development of sinistral strike-slip to normal dip-slip N-S- to NNE-SSW-trending faults (e.g. [5, 13, 26, 30, 31]). These structures have been described from numerous coastal exposures including north of Caithness (e.g. [4, 5, 13]—their Group 1 structures), east of Caithness at Sarclet (Figure 1; [21]), and from the southern coastal region of the Inner Moray Firth Basin in the Turriff SubBasin (Figure 1; [19]).

These Devonian rift-related structures are locally reactivated during a regionally recognized phase of E-W compression, leading to the development of N-S-trending folds and thrusts (e.g. Group 2 structures of [4, 5], see also [32–35]). These structures are widely considered to be Late Carboniferous—Early Permian and are thought to be associated with the dextral strike-slip reactivation of the Great Glen Fault, possibly due to the westerly extrusion of NW Europe following closure of the Ural Sea or—perhaps less likely—to the far-field effects of the Variscan orogenic event (e.g. [13, 26, 31, 36]).

To the N of the Helmsdale Fault, the Devonian and Permo-Carboniferous structures in north Caithness and Orkney are widely overprinted by dextral oblique NE-SW-striking faults and sinistral E-W- to ENE-WSW-striking faults with widespread syn-deformational hydrothermal carbonate-base metal sulfide and hydrocarbon mineralization (Group 3 structures; [5, 35]). Re-Os geochronology of vein-hosted pyrite in northern Caithness yielded ages of c. 267 Ma [14] and is considered to related to the Permo-Traissic formation of the West Orkney Basin (Figure 1), located offshore to the north of Scotland. In eastern Caithness, at Sarclet (Figure 1), mm- to cm-wide N-S-trending calcite veins have been identified, which yielded an absolute U-Pb date of c. 258–255 Ma (Late Permian; [21]). These fractures are either far-field manifestations of the West Orkney Basin rifting and/or are related to early rifting in the Central/Viking graben of the North Sea [21].

Events younger than the Permian have not been widely documented in the north Caithness or Orkney area (e.g. [5, 14, 35]).

2.2. Superimposed Mesozoic-Cenozoic Events

The Devonian strata in eastern Caithness and Turriff Subbasin preserve structures related to the later Mesozoic-Cenozoic opening [19, 21] and inversion of the Inner Moray Firth Basin [21]. The Late Jurassic–Early Cretaceous rifting which led to the opening of the regional-scale basin is widely characterized by the development of kilometer-long, predominantly NE-SW-trending growth faults [16]. The most prominent structures onshore known to be associated with this event are the sinistral transtensional Helmsdale Fault (c. 159-115 Ma) and dextral splay related to the Great Glen Fault at Shandwick (c. 123 Ma; U-Pb calcite ages from [22]). In addition, in the Devonian strata at Sarclet (Figure 1), dip-slip to normal-sinistral oblique E-W- to NE-SW-trending faults are associated with syn-tectonic calcite mineralization that yielded U-Pb ages of c. 134 Ma [21].

Kemp et al. [37] used K–Ar dating of fault gouges linked to the onshore Sronlairig Fault (Figure 1), which is an ENE-WSW-trending sinistral fault associated with the GGF. This revealed two distinct ages of movement and gouge deformation: Late Carboniferous–Early Permian (c. 296 Ma) and Late Jurassic–Early Cretaceous (c. 145 Ma). The latter age is thought to be associated with a relatively late movement along this fault during the opening of the Inner Moray Firth Basin. Further to the east, in the Turriff Subbasin (Figure 1), the Devonian N-S to NNE-SSW trends are also locally dextrally reactivated during NW-SE extension. Associated syn-faulting carbonate mineralization here has yielded Early Cretaceous ages (c. 131 Ma; [19]).

The structures associated with the Latest Cretaceous- to Cenozoic-age regional uplift, tilting and faulting in the Inner Moray Firth Basin are not yet confirmed by absolute dating. However, strike-slip fault arrays observed at Sarclet are inferred to be Cenozoic and related to the dextral reactivation of the GGF offshore [21, 38]. More widely, Cenozoic reactivation of previously formed major NE-SW- to E-W-trending fault complexes in the Inner Moray Firth Basin has been recognized offshore (e.g. the Lossiemouth Fault zone, [20]). Onshore along the southern margin of the basin, oblique dextral reactivation of E-W- to ENE-WSW-trending faults (e.g. Clashach Cove Fault, [20]) is associated with widespread iron oxide mineralization. All of these Cenozoic events may be related to broadly ESE-WNW compression due to the far-field effects of North Atlantic spreading [39].

3. METHODOLOGY

Structural fieldwork and sampling were carried out in Devonian rocks located along the northern coastal sections

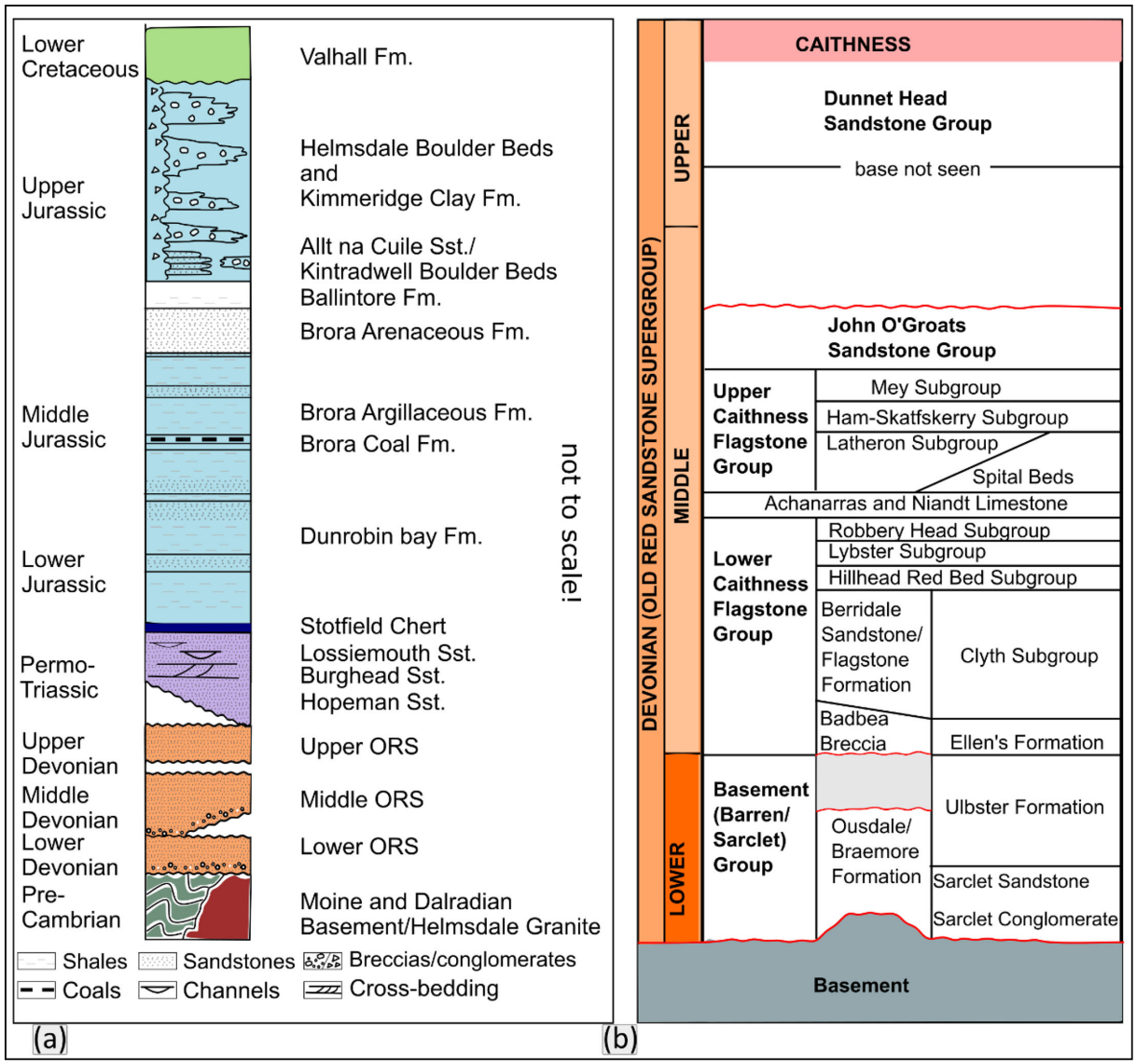

FIGURE 2: Summary of (a) onshore stratigraphy of the Inner Moray Firth Basin, not to scale, with notional relative thicknesses shown. ORS—Old Red Sandstone. (b) Detailed stratigraphy of the Devonian/Old Red Sandstone sequences onshore. Taken from [21]—compiled after [17, 58–60].

of the Inner Moray Firth Basin at Berridale and Whaligoe (Figure 1). These areas lie in the footwall of the Helmsdale Fault which is located c. 1–2 km offshore. Grid references used in this article refer to the British National Grid. Detailed observations and structural measurements were recorded during fieldwork. For structural data processing and visualization, we used Stereonet 10 software (lower hemisphere, equal-area projections; [40]). Fault-slip slickenline data were collected in the field to perform palaeostress inversions. For that, we used the direct inversion method (INVD) of Angelier [41] implemented using the SG2PS software [42]. UAV aerial imagery was captured utilizing a DJI Mavic Air drone. Agisoft Metashape Professional™ (v.1.6.2) was employed for the creation of the digital outcrop models (DOM) and orthorectified models following the workflow detailed in Tamas et al. [43]. The DOM are published on the Sketchfab repository (see Supplementary Material section for details and links). The orthorectified models were overlapped onto the aerial maps obtained using the EDINA Digimap service. This service provides access to high-quality 25 cm vertical ortho-photography available for Great Britain, created and licensed by Getmapping PLC.

Fault rocks including calcite-filled fault and fracture (vein) samples were collected for microstructural and geochronology studies. Polished chips or thick sections of the calcite-mineralized veins were analyzed using laser ablation–inductively coupled plasma–mass spectrometry at the University of Hull (UK). The calcite U-Pb geochronology methods described in Holdsworth et al. [44] were employed for the analysis process. Data were processed using Iolite v4, with the VisualAge U-Pb DRS. Analytical conditions and data are provided in the (Online Supplementary Material Appendix A). The calcite samples

are characterized by variable sample to sample U and Pb concentrations (sample averages of U and Pb concentrations respectfully for each sample are: B01 2.08 and 6.03 ppm; B03 4.45 and 2.32 ppm; BD10 2.05 and 8.33 ppm; WS05e 0.58 and 1.10 ppm; and WS05l 2.10 and 11.59 ppm). Data with analytical uncertainties larger than typical for each sample or with significant outliers were not utilized in the final calculation. The ages are calculated as lower intercept $^{238}U/^{206}Pb$ ages with uncertainties quoted at 2 seconds and include propagation of systematic uncertainties; these incorporate the analytical uncertainties of the WC1 reference material during each session and a conservative estimate of long-term reproducibility of 2% for NIST612. Initial Pb compositions (upper intercepts) are provided in the summary table in Online Supplementary Materials Appendix A. All data plotting and age calculations used IsoplotR [45], and ellipses represent 2 seconds uncertainties.

4. RESULTS

4.1. Field Observations and Sample Locations

4.1.1. Berridale [Grid Reference: ND 12195 22654]

The Berridale outcrops are located in the steep but accessible coastal sections ~300 m east of Berridale village [ND 117 227] (Figure 3(a) and 3(b)). The investigated exposure is c. 600 m long and is formed almost entirely of high cliffs (30, 80 m high) and narrow rock platforms, some of which can be accessed at mid to low tide. A large orthomosaic (Figure 3(b)) and 3D model (Figures 4(a) and 4(b)) across the entire area was obtained using the UAV to enable data visualization, interpretation, and display, as large portions of the outcrop are inaccessible on foot. The Berridale Flagstone Formation of the Lower Caithness Flagstone Group (Middle Devonian, Figure 2) crops out here (Figure 3(a); [46]) and comprises predominantly cm- to dm-thick beds (about 5 to 50 cm) of laminated gray mudstones and fine laminated red/brown and gray sandstones. These deposits have previously been interpreted as a low-energy, fluvial-lacustrine sequence laid down on the southwestern margin of the Orcadian basin [47]. The bedding is mostly shallowly dipping to the ESE (Figure 3(c)).

Two sets of faults and fractures are dominant in the outcrops shown in Figure 3(b). The first set are ENE-WSW- to NE-SW-trending, moderately to steeply dipping predominantly to the NW, while the second dominant set are NNW-SSE- to NW-SE-trending, moderately to steeply dipping to the WSW (Figure 3(d)). The cliffs on the northern side of the exposure (Figure 4(a)) could not be accessed on foot, and measurements were made based on the 3D outcrop using VRGS software. Mainly, NNW-SSE- to NW-SE-trending faults can be observed at this location, steeply dipping to the WSW/SW. Toward the eastern side of the outcrop, a NW-SE-trending fault crosscuts through the stratigraphy dipping at a lower angle (c. 40º; shown in pink in Figure 4(a)). Here, the strata are locally folded in its hangingwall and footwall (Figure 4(a)), suggesting at least a component of reverse movement (top-to-the-NE). In the lower part of the cliff, the fault links into a preexisting steeper normal fault, which is interpreted to have been compressionally reactivated and shortcut by the reverse fault oriented at a lower angle (Figure 4(a)).

On the southwestern side of the cliff section close to the beach (Figure 4(b)), a wide deformation zone of about 5 m can be accessed directly. In the deformation zone, N-S- to NNW-SSE-trending faults moderately dipping to the W are well exposed. These faults are nonmineralized and are associated with fault breccia and locally developed deformation bands with millimeter to centimeter normal displacements based on offset bedding (Figure 4(c)). The fault planes of these N-S- to NNW-SSE faults show dip-slip lineations (Figure 4(d)). The strata in the hangingwall show gentle thickening toward the fault (Figures 5(a) and 5(b)). In the fault hangingwall, some NNW-SSE-trending, m-scale folds, and small-scale (cm- to dm-scale) folds and thrusts (Figure 5(c)) are developed. These observations may suggest that the earlier formed normal growth faults have been later compressionally reactivated during a later phase of ~ E-W shortening.

On an exposed bedding plane an array of mm-thick N-S-trending white calcite tensile veins are observed (Figure 5(g)). These veins, limited to this exposure, are the only veins of this type and orientation identified in the local studied area.

The N-S- to NNW-SSE-trending faults and folds are then crosscut by a set of ENE-WSW- to NE-SW-trending faults and fractures (Figures 5(a) and 5(b)). The cliff face of this outcrop above the beach represents such a fault plane (Figure 5(b) shown in green). Some of these fault planes are heavily iron oxide-stained (Figure 5(c)) and are associated with iron oxide–stained fault breccia and mm-thick white/yellow calcite tensile veins (Figure 5(d)). Two differently oriented kinematic indicators are preserved on the fault plane, suggesting two episodes of movement. The earlier episode is associated with normal, slightly sinistral oblique-slip slickenlines and calcite slickenfibers (Figure 5(d); pitches between 70 and 82 SW), while the later event is associated with dextral-normal oblique-slip slickenlines (pitches between 46 and 52 NE) observed on the iron oxide films (Figure 5(c)). Two samples were selected from this fault plane, one from the iron-mineralized fault breccia ($B0_2$) and one sample from the tensile calcite vein ($B0_3$) (Figure 5(d)).

Other ENE-WSW- to NE-SW-trending faults in the area are associated with calcite mineralized fault breccias up to 20 cm wide (Figure 5(e)) or 10–15 cm wide mineralized fracture zones made up of clusters of mm-thick white veins of calcite and fine, red-colored sediment infills (Figure 5(f)). Both types of structures were sampled for microstructural study and dating (B10—from the calcite mineralized breccia and B01 from the thin veins with red sediment infills).

4.1.2. Whaligoe [Grid Reference ND 32140 40249]

The Whaligoe locality lies ~200 m south of Whaligoe village [ND 320 404] (Figures 6(a) and 6(b)). The investigated

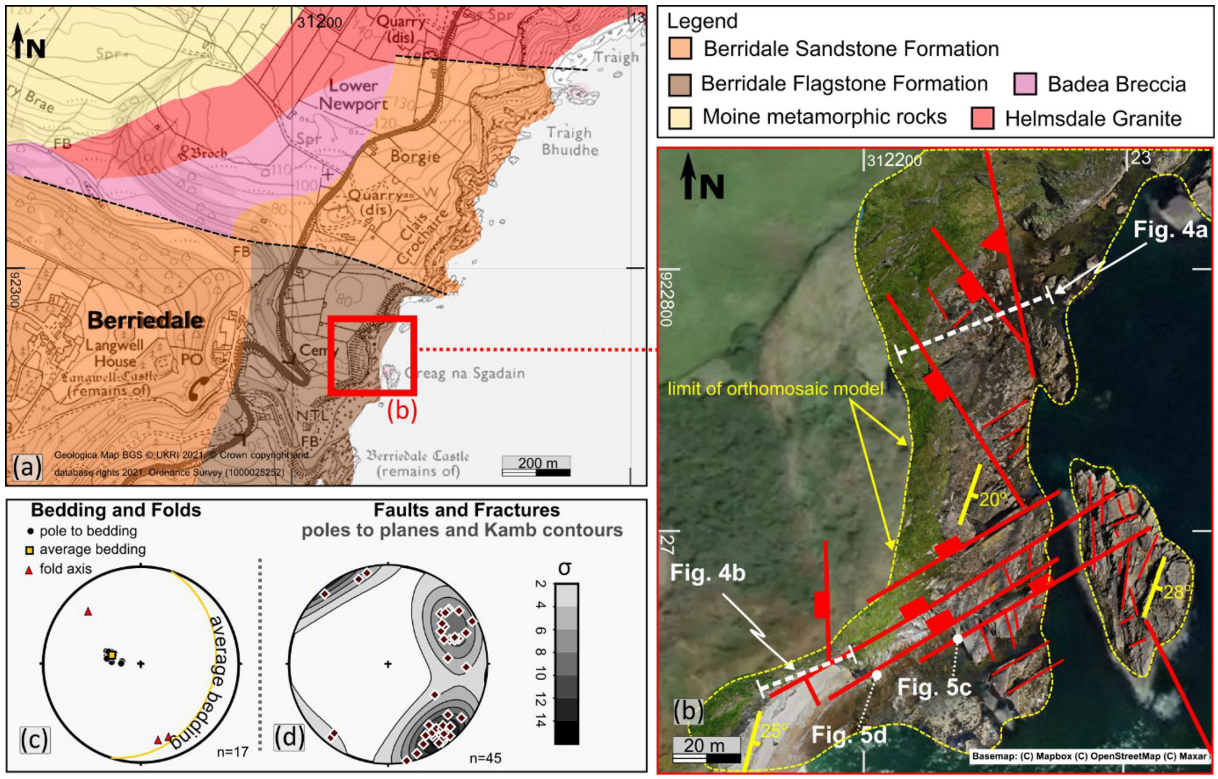

FIGURE 3: (a) Geological map of Berridale area (using EdinaDigimap service and [46]) showing the location of (b) orthomosaic model obtained from UAV (Unmanned Aerial Vehicle) photography overlapped on aerial map (using EdinaDigimap service © Getmapping PLC) of the studied exposure showing the main structural trends. Approximate orientation of Figures 4(a) and 4(b) is also indicated by the white dashed line. (c,d) Stereonets of structural data collected in the field. Lower hemisphere, equal-area projections.

exposure is formed almost entirely of steep cliffs (about 50-60 m high), the bottom of which can be accessed at lower tides using the "Whaligoe Steps" (Figure 6(b)). A large 3D model across the entire area was obtained using the UAV to enable data visualization, interpretation, and display (Figure 6(c)), especially since most of the cliffs are inaccessible on foot. The Middle Devonian Whaligoe Formation of the Clyth Subgroup (Figures 2 and 6(a)) [46] is well exposed in the high cliffs and very narrow, flat-lying rock platforms below. The succession comprises predominantly mm- to cm-thick beds (of about 5 mm to 10 cm) of light to dark gray alternating fine sandstones, siltstones, and mudstones. Symmetrical ripple marks (Figure 6(g)) and subaerial desiccation cracks are widespread on exposed bedding planes. This succession has been interpreted as shallow lake mudflats with some stream/river influx deposits, part of the larger Orcadian Lake (e.g. [48]).

The bedding at this location is mostly subhorizontal to shallowly dipping to the SW (Figure 6(d)). The succession is intensely fractured and faulted by two dominant sets of structures. The first set are ESE-WNW-trending, dipping moderately to vertical predominantly to the SSW, while the second dominant set is NE-SW- to ENE-WSW-trending, dipping from moderately to vertical both to the SE/SSE and NW/NNW (Figure 6(e)). Subordinate sets of N-S-, NNW-SSE-, and NNE-SSW-trending faults also occur, mostly visible higher up in the cliffs (Figure 7(a)). The N-S, NNW-SSE trends (Figures 7(a) and 7(b) in dark red) appear to be crosscut by the NNE-SSW-trending fault (Figures 7(a) and 7(b), planes shown in bright red).

These sets are all crosscut by ESE-WNW- and NE-SW- to ENE-WSW-trending faults (Figures 7(a) and 7(b) in green). The later faults are associated with well-developed fault cores formed either by a cohesive fault breccia between 20 and 50 cm thick (Figures 7(c) and 7(d)) or by a c. 3–4 m-wide shear zone with multiple strands of fine-grained gray and yellow fault gouge (Figure 8(a)). Highly boudinaged sandstone beds can be observed strung out along these fault zones (Figure 8(a)). Immediately next to this fault core, a damage zone 2–3 m thick occurs in which there is extensive calcite veining. Multidirectional calcite veins (submillimeter to millimeter), tension gashes, calcite-cemented explosion breccias and mm to c. 5 cm wide tensile veins with jigsaw-like inclusions of Devonian host rock (Figures 8(b)–8(d)) occur. These mineralized structures could represent local explosive hydrofractures synchronous with faulting. One sample from such a mineralized feature, Ws05, was selected for microscopy and geochronology (Figure 8(c)).

The ENE-WSW-trending subset, which preserves better-exposed fault planes, shows a significant component of normal movement based on offsets of bedding markers and kinematic indicators showing dip-slip lineations and grooves on the slip planes (e.g. Figures 7(d) inset and Figure

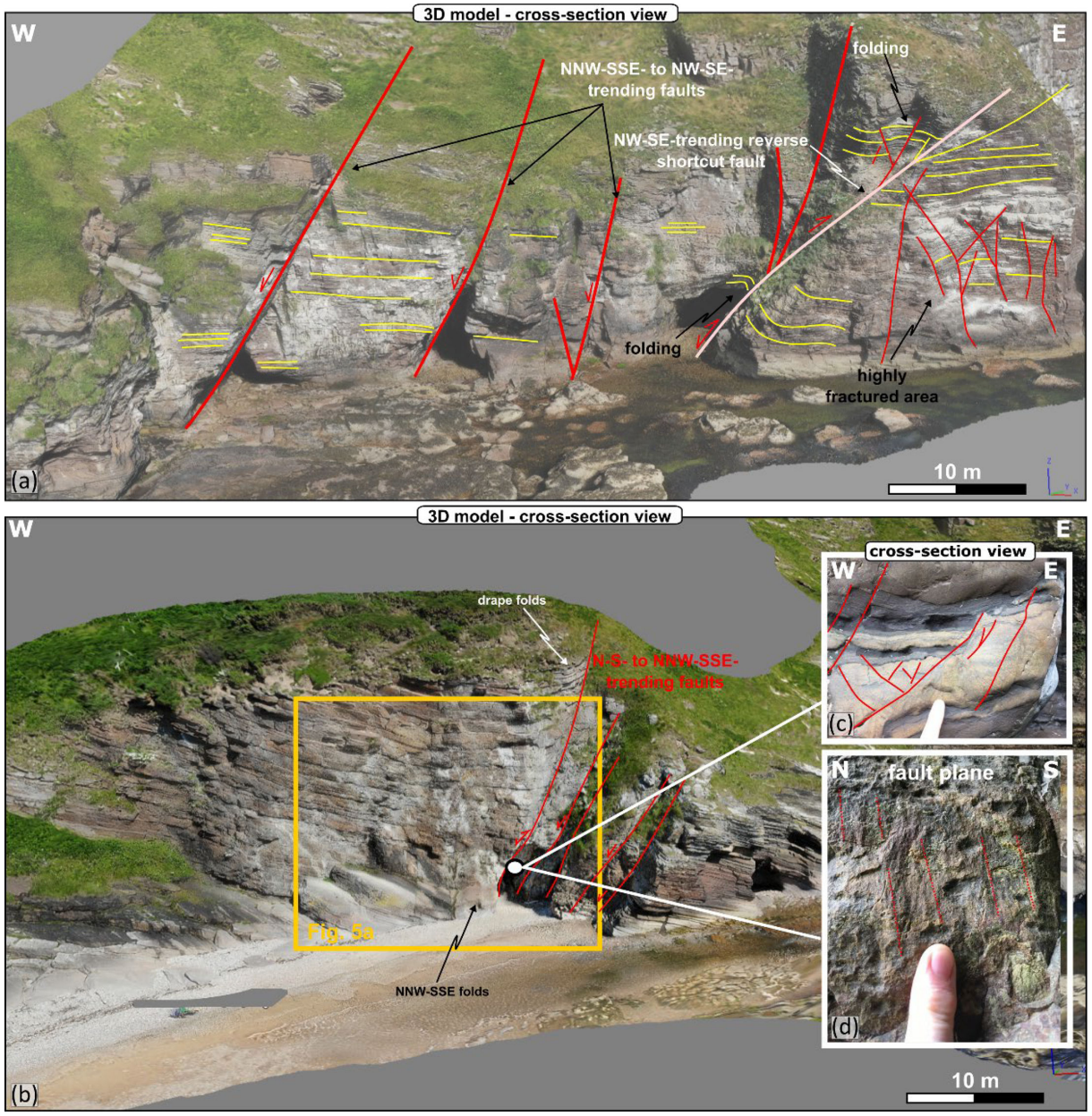

FIGURE 4: 3D digital outcrop models of (a) the cliffs in the northern part of the exposure showing faults and folds occurring at Berridale and (b) the cliffs in the southern part of the exposure at Berridale (see location on Figure 3) (c) field photograph showing the deformation bends associated with the N-S-trending fault zone, and (d) dip-slip kinematics observed on the main fault plane.

8(e)). A palaeostress inversion analysis of the slickenline lineations associated with these faults yields an NNW-SSE extension direction (Figure 8(f)).

4.2. Microscopy

4.2.1. Berridale

The B10 sample (Figure 9(a)) was collected from an ENE-WSW-trending fault associated with calcite mineralized fault breccia (Figure 5(e)). It represents a relatively "clean" sparry calcite-filled jigsaw breccia with syntaxial growth patterns and local development of zoning defined by dusty inclusion trails and small intergrown grains of pyrite (Figure 9(b)). In places, there is also evidence of an earlier sparry calcite fill postdated by a pale brown calcite-cemented sediment fill (Figure 9(c)). Both of these were then brecciated by the later calcite fill; both sediment and calcite fill carry sparse pyrite, but not the Devonian host (Figure 9(c)). Some areas of zoned fill show later fracturing and possible later sediment or iron oxide fills (Figure 9(d)).

The B01 sample (Figure 9(e)) was taken from a NE-SW-trending fault zone (Figure 5(f)) comprising an irregular network of fine-grained red sediment fills with patches of calcite fill/veins often hosted in the same fracture (e.g. Figure 9(f)). Sediment fills are generally earliest and rich in iron oxide (limonite, but not hematite). Other minerals

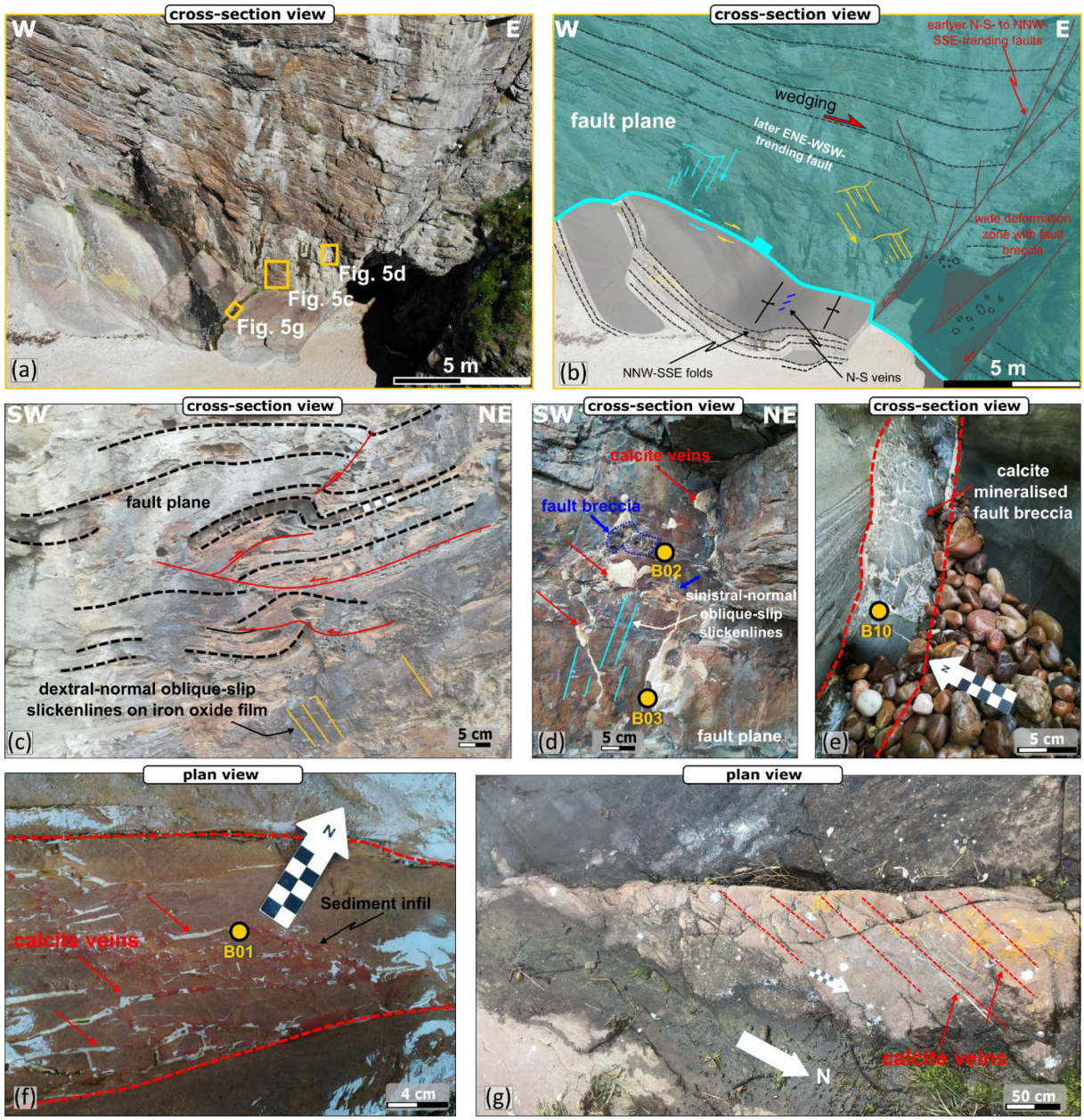

FIGURE 5: (a) Field photograph and (b) line drawing showing the crosscutting relationship between the sets of structures recognized at Berridale. Location of (c, d, and g) are indicated on (a). (c) Field photograph showing the ENE-WSW-trending fault plane at Berridale. Note the small-scale fold and thrusts in the Devonian layers intersected by the fault; however, these might be soft-sediment features. Dextral oblique-kinematics can be observed on the Fe-oxide mineralized fault plane (yellow lines). (d) Field photograph showing the sinistral oblique kinematics (blue lines) on the same ENE-WSW-trending fault plane as well as fault breccia and calcite mineralization associated with the fault. Location of samples B03 and B02 are indicated on the image. (e) ENE-WSW-trending fault associated with calcite-mineralized fault breccia. Location of B10 sample is indicated on the image. (f) ENE-WSW-trending fault zone with tensile calcite veins and red-colored sediment fill. Location of sample B01 is indicated on image. (g) En-echelon N-S-trending calcite veins.

present include rare patches of pyrite (Figure 9(g)) and flakes of colorless low relief zeolite (Figure 9(h)), both of which are intergrown with calcite. The pyrite markedly darkens the color of the local sediment fill (Figure 9(f)). The fractures in the B01 sample trend at various angles to bedding in the fine-grained host Devonian sandstone and commonly display geopetal filling geometries, all giving consistent younging sense relative to bedding in host rocks (Figure 9(i)).

The B03 sample (Figure 10(a)) was taken from an ENE-WSW-trending fault plane (Figure 5(d)) and represents a composite tensile sparry calcite vein with syntaxial growth, with at least three texturally distinct fills (Figures 10(b) and 10(c)). Earlier phases are generally

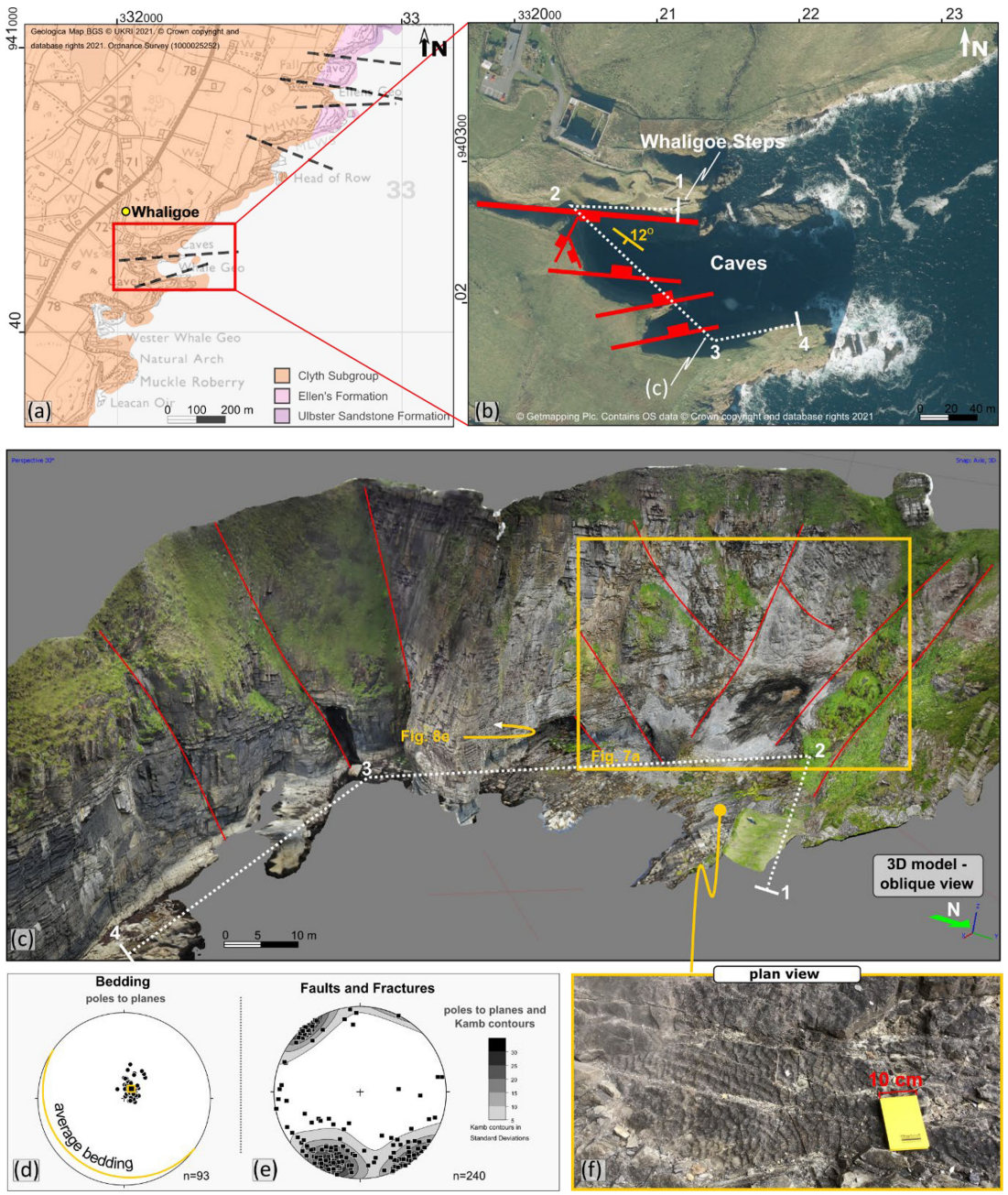

FIGURE 6: (a) Geological map of Whaligoe Steps area (using EdinaDigimap service and BGS 1985) showing the location of (b) aerial map (using EdinaDigimap service © Getmapping Plc) of the studied exposure showing the main structural trends. Approximate orientation of (c) is also indicated by the numbered white dotted line. (c) 3D digital outcrop model of the cliff exposure with location of (g) and Figures 7(a) and 8(e) indicated on the image. (e,f) Stereonets and rose plots of structural data collected in the field. Lower hemisphere, equal-area projections. (g) bedding surface with ripples.

zoned, inclusion rich, including hydrocarbons (Figures 10(c) and 10(d)), while later fills are clean, sparry calcite locally intergrown with hematite (Figure 10(c)). In addition, a later fracture with irregular, cataclastically deformed calcite (Figure 10(e)) with deformation twins in the surrounding vein material (Figure 10(e)) can be observed. This may indicate a later, minor shearing event.

The B02 sample (Figure 11(a)) was collected from the same ENE-WSW-trending fault plane as B03 (Figure 5(d)). This sample is hematite-rich and noticeably calcite-poor, comprising a partially cemented vuggy breccia, with large clasts (mm to cm) of Devonian sandstone wall rocks. The porous hematite cement (Figure 11(b)) shows widespread marginal alteration to limonite, possibly due to weathering in the open cavities (Figure 11(c)). Small areas of earlier sediment fills (like those seen in sample B01—see below) are preserved locally and are postdated by brecciation and hematite fills (Figure 11(d)). Many open cavities are lined with thin rinds of orange-brown fibrous speleothem/travertine possibly formed due to relatively recent mineral

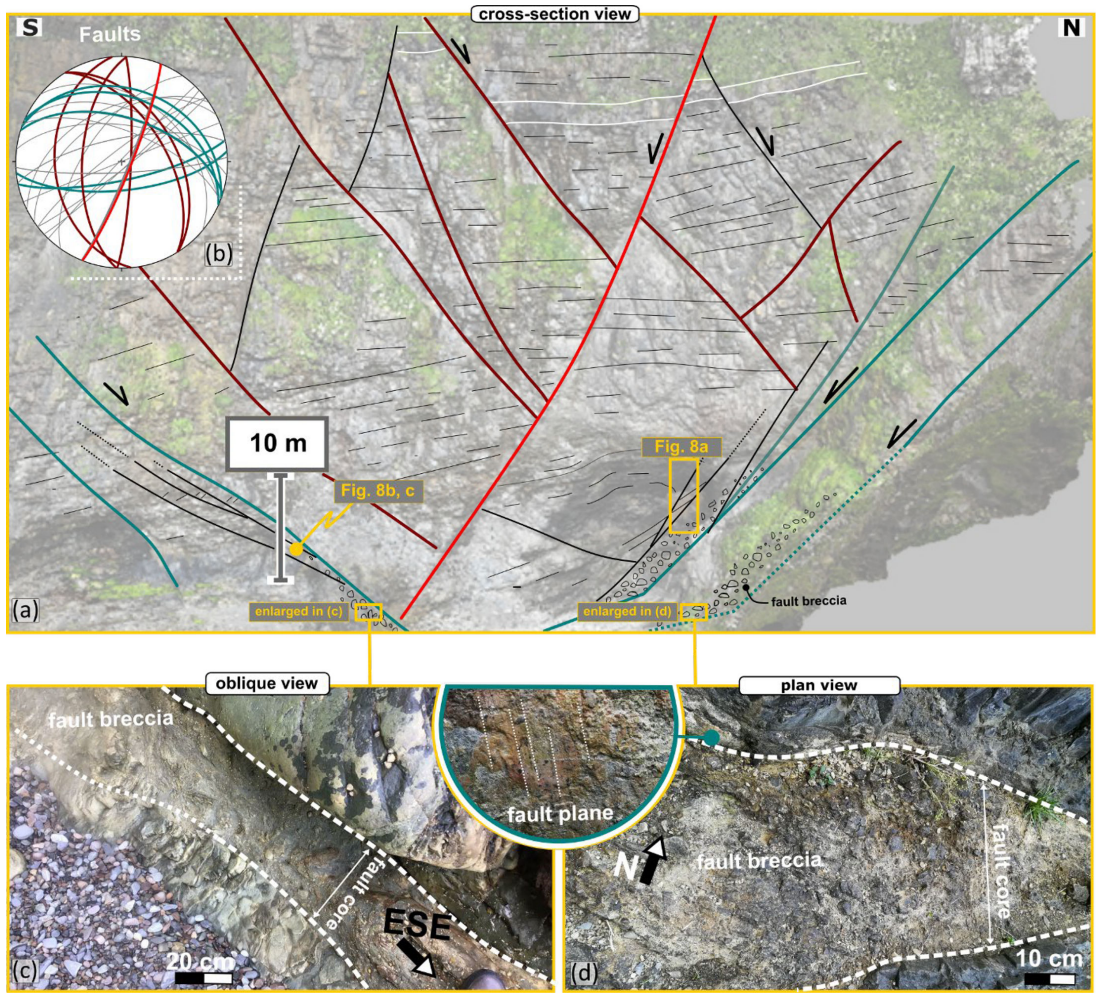

FIGURE 7: (a) Detailed interpretation of fault networks on the N-S-trending cliff face (see location at Whaligoe Steps on Figure 6(c)) and (b) Stereonet showing the orientation of visible faults in (a) in the same colors. Faults in green are ENE-WSW- to ESE-WNW-trending and are crosscutting the red and brown NNW-SSE- to NNE-SSW-trending faults. These later faults are associated with fault breccia (c,d), gouge (see Figure 8(a)) and calcite mineralization (see Figures 8(b)–8(d)). (c,d) Field photographs showing fault breccia in the fault core of the faults shown in (a) and (d) (inset) dip-slip/slightly oblique-sinistral slickenlines on the exposed slip planes.

precipitation in open cavities (Figures 11(e) and 11(f)). A silicified echinoderm stereom (Figure 11(g)) (implying a marine input) and other possible microfossils, including circular and angular shell fragments (Figure 11(h)), are locally preserved in the fracture fill.

4.2.2. Whaligoe

The Ws05 sample (Figure 12(a)) was taken from the fault-parallel vein set (Figure 8(c)) closely associated with the major ENE-WSW-trending fault illustrated in (Figure 8(a)). These veins are white and translucent in outcrop and hand specimen with large sparry calcite crystals surrounded by a finer grey matrix/cement (Figure 12(a)). Thin sections were cut both normal to the vein (Figures 12(b) and 12(c)) and at low angles to the vein walls (Figures 12(d)–12(g)) to better investigate both the sparry crystals and the finer fill. Two distinct fills are visible in thin sections. An earlier sparry zoned calcite with local intergrown pyrite crystals, and a later "dusty," inclusion-rich, fine-grained carbonate fill with local large calcite overgrowths (e.g. Figures 12(b) and 12(c)). These are sometimes formed in optical continuity with the older sparry calcite crystals (Figure 12(c)).

The younger fill is interpreted as a fine-grained carbonate-cemented sediment (Figures 12(h) and 12(i)). It appears to infill vuggy cavities lined by early fill sparry zoned calcite crystals (e.g. Figure 12(e)) and contains many fine clastic inclusions, including carbonate and iron oxide clasts (Figures 12(j) and 12(k)).

4.3. Geochronology

Three samples from Berridale (Figures 9(a), 9(e), and 1(a)) contained sufficient amounts of ^{238}U (and low enough concentrations of common Pb) to yield accurate and precise dates.

For sample B10, 132 ablation spots were plotted on a Tera-Wasserberg U-Pb plot using IsoplotR, which yielded a

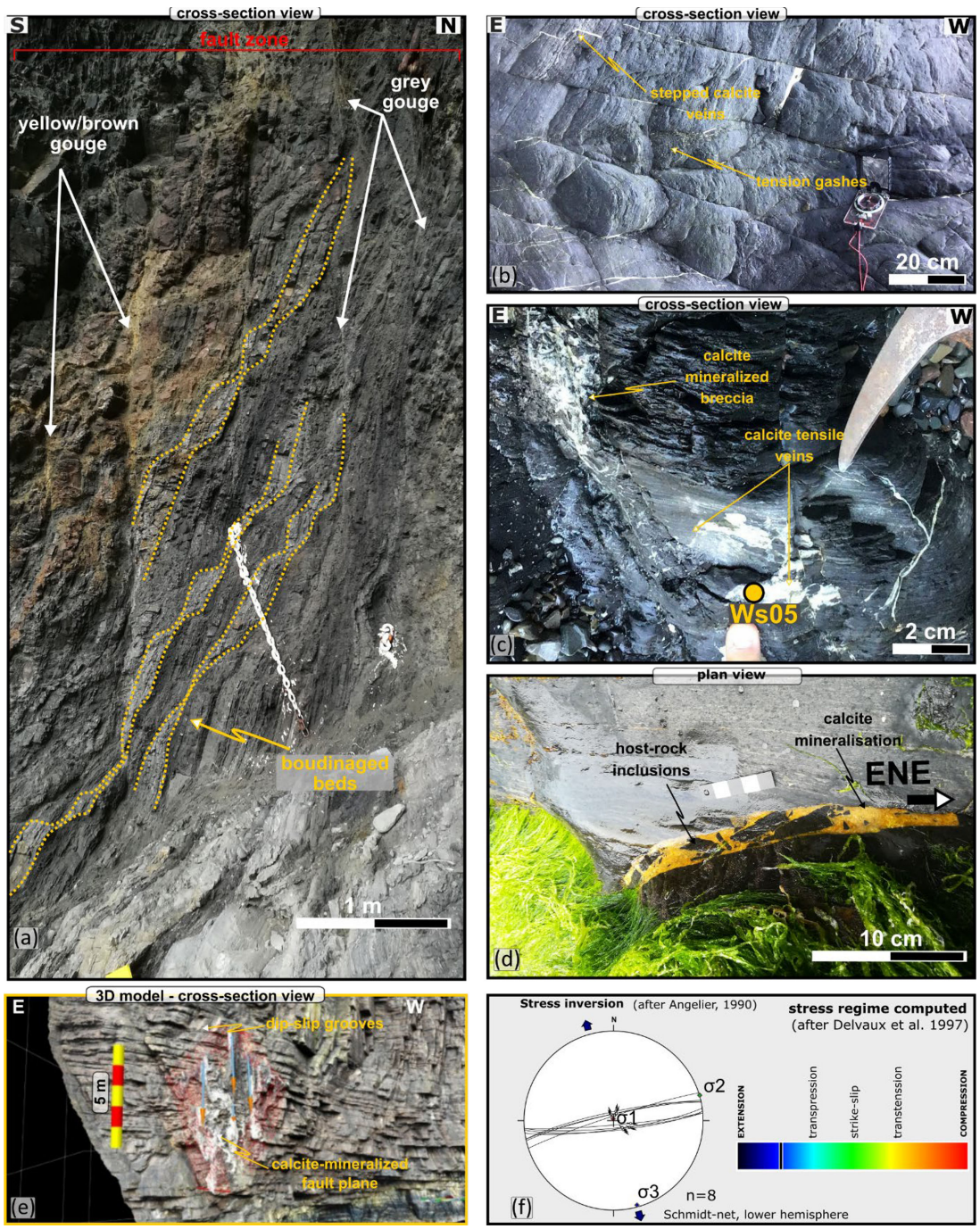

FIGURE 8: (a) Field photograph showing a c. 3 m wide fault zone associated with a ENE-WSW-trending fault (see location at Whaligoe Steps on Figure 7(a)) showing multiple strands of fault gouge. (b–d) calcite mineralization associated with the ESE-WNW-trending fault shown in (a). The location of sample Ws05 is indicated on (b). (e) detail from 3D digital outcrop model showing an E-W-trending fault plane with dip-slip grooves. (f) Stress inversion plot (after [41]) of fault lineation data.

$^{238}U/^{206}Pb$ age of 151.66 ± 5.09 Ma (2σ, $Pb_{initial}$ = 0.8299 ± 0.0055, MSWD = 0.4.9; Figure 13(c)).

For sample B01, 198 ablation spots were plotted on a Tera-Wasserberg U-Pb plot using IsoplotR, which yielded a $^{238}U/^{206}Pb$ age of 148.83 ± 6.12 Ma (2σ, $Pb_{initial}$ = 0.7780 ± 0.0233, MSWD = 35; Figure 13(a)).

For sample B03, 234 ablation spots were plotted on a Tera-Wasserberg U-Pb plot using IsoplotR, which yielded a $^{238}U/^{206}Pb$ age of 147.01 ± 2.48 Ma (2σ, $Pb_{initial}$ = 0.8010 ± 0.0049, MSWD = 3.4; Figure 13(b)).

For the sample collected at Whaligoe (Figure 12(a)), the ^{238}U and ^{206}Pb concentrations were analyzed in both early sparry fill (Ws05e) and later fine fill (Ws05l). Both analyzed zones contained sufficient amounts of ^{238}U (and low enough concentrations of common Pb) to yield accurate and precise dates.

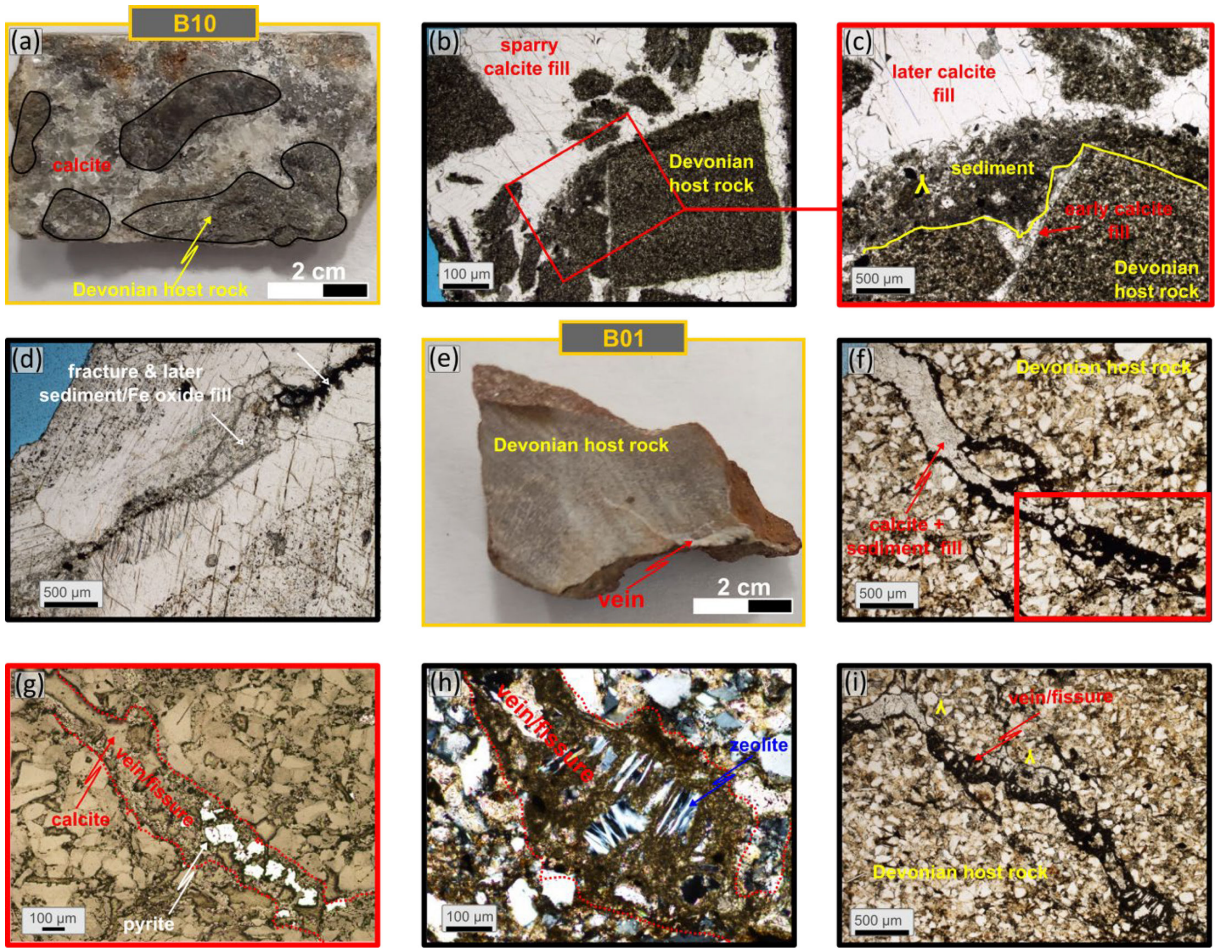

FIGURE 9: Samples and microstructures associated with calcite mineralization at Berridale 1. (a) Hand specimen of the B10 sample (b) thin section microphotographs showing a relatively "clean" sparry calcite-filled jigsaw breccia with syntaxial growth patterns and (c) local development of zoning defined by dusty inclusion trails and small intergrown grains of pyrite (d) later fracturing and possible later sediment or Fe Oxide fill. (e) Hand specimen of B01 sample showing (f) an irregular network of fine-grained red sediment filled with patches of calcite fill/veins and (g) rare patches of pyrite, (h) flakes of colorless low relief zeolite both of which are intergrown with calcite, (i) geopetal filling geometries.

For sample Wa05e, 136 spots were ablated and were plotted on a Tera-Wasserberg U-Pb plot using IsoplotR, which yielded a $^{238}U/^{206}Pb$ age of 154.4 ± 28.8 Ma (2σ, $Pb_{initial}$ = 0.804 ± 0.014, MSWD = 1.6; Figure 13(d)).

For sample Wa05l, 290 spots were ablated and were plotted on a Tera-Wasserberg U-Pb plot using IsoplotR, which yielded a $^{238}U/^{206}Pb$ age of 19.32 ± 10.82 Ma (2σ, $Pb_{initial}$ = 0.8169 ± 0.0020, MSWD = 2; Figure 13(e)).

5. DISCUSSION

The N-S- to NNW-SSE-trending faults (e.g. Figures 4(a), 4(e), 7(a), and 7(b)) appear to represent the earliest structures observed at both at Berridale and Whaligoe. At Berridale, these faults show evidence of normal dip-slip and stratal thickening in their hangingwall (Figures 5(a) and 5(b)), suggesting syn-kinematic growth faulting during deposition of the Berridale Formation (Middle Devonian; Figure 2). Faults with such orientations have been widely documented across the Orcadian Basin in both Caithness and on the southern margin of the IMFB (see [5, 13]—their Group 1 structures; [20]). These faults are interpreted to be associated with the sinistral shear along the Great Glen Fault zone leading to transtensional opening of the Orcadian Basin during the Early-Middle Devonian [13, 26, 30, 31].

N-S- to NNW-SSE-trending reverse faults and folds (e.g. Figure 4(a)) are most likely inverted earlier Devonian structures, contemporaneous with the compressional structures also observed at Sarclet, some 3 km to the northeast of Whaligoe (Figure 1; [21]) and elsewhere from the Scottish mainland to Shetland (e.g. [4, 5, 33–35, 38]). These structures are therefore correlated with the Group 2 structures of Dichiarante et al. [5] and are interpreted to have formed in association with dextral strike-slip reactivation of the Great Glen Fault which lies a few kilometeres offshore of the present study areas (e.g. [4, 5, 13, 26, 31, 35, 36]).

The en-echelon mm-thick N-S-trending calcite tensile veins seen at Berridale (Figure 5(g)) are similar in terms of orientation and mineralization to the N-S-trending calcite

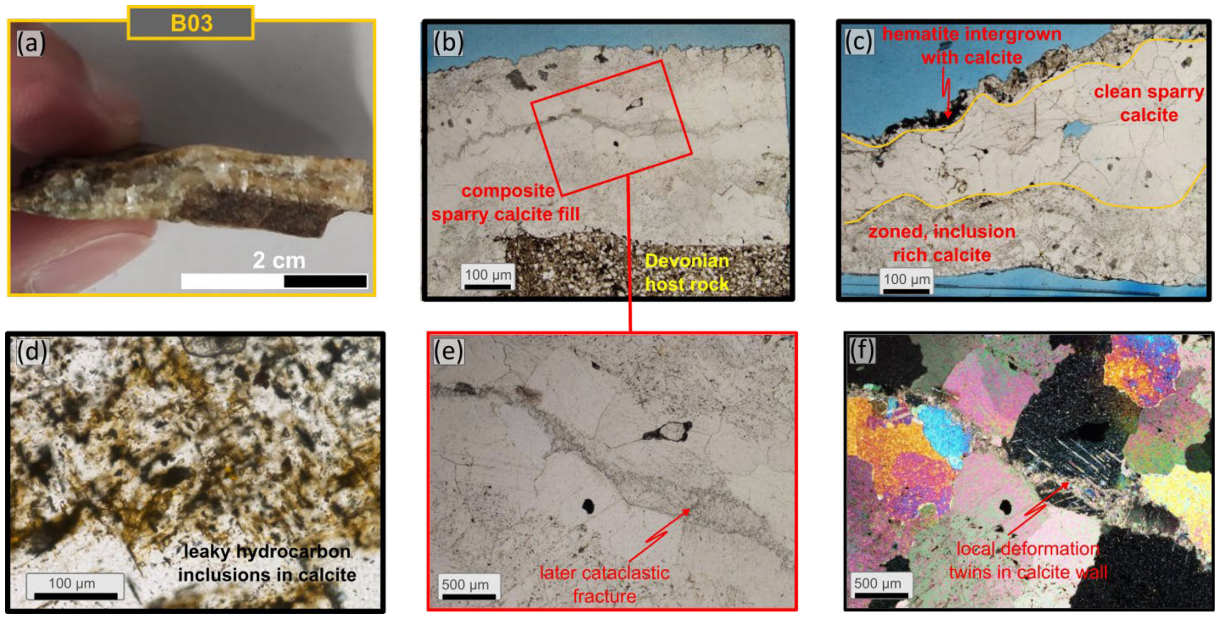

FIGURE 10: Samples and microstructures associated with calcite mineralization at Berridale 2. (a) B03 hand specimen of calcite vein. (b–f) Representative thin section microphotographs of B03 sample showing (b,c)—plane polarized light) composite sparry calcite fill with light [(d) plane polarized light] hydrocarbon inclusions and [(e) plane polarized light] later cataclastic fracture with [(f) crossed polarized light] local deformation twins in the calcite wall.

veins of Permian age (c. 258 Ma) observed at Sarclet [21]. Likely, these veins are also Permian. In northern Caithness, they are interpreted to be associated with the opening of the West Orkney Basin offshore and to the north of Scotland [5, 14]. In most of the Inner Moray Firth Basin, the Permo-Triassic history is characterized by subsidence and passive infill of the Variscan palaeotopography (see [20] for more details). However, Permo-Triassic rifting is recognized further to the east in the Central/Viking graben, during E-W extension (e.g. [49]). Thus, the early N-S calcite veins at Berridale may well be the far-field products of Permian rift episodes centered to the north and/or east of the later Inner Moray Firth Basin.

The NNE-SSW- to NNW-SSE-trending faults and folds are then crosscut by later NE-SW- to ESE-WNW-trending faults and fractures (e.g. Figures 3(b), 5(b), and 7(a)). These faults are consistently associated with calcite mineralization (Figures 5(d) - 5(f), 8(b),- 8(d)) and most likely represent a polymodal set of faults (fractures) formed simultaneously (e.g. [50, 51]). In Berridale, these faults show evidence of two episodes of movement. A normal sinistral oblique-slip event, widely associated with calcite mineralization, and a later normal-dextral oblique-slip event. This later event is associated with iron-oxide mineralization as concluded from field observations and thin section (e.g. Figures 5(c), 5(d), and 11).

As revealed by the geochronology, the timing of the calcite mineralization associated with the NE-SW- to ENE-WSW-trending structures is (within error) Kimmeridgian-Tithonian (Figure 13). These fault orientations correlate well with the offshore structures associated with the opening of the Inner Moray Firth Basin (e.g. [16, 20]), and their timing falls within the main Late Jurassic–Early Cretaceous syn-rift episode, which led to the opening of the basin (e.g. [16, 52]). These fault orientations are also parallel to other Devonian-hosted ESE-WNW-trending faults visible on the geological map (Figures 3(a) and 6(a)), but we can only infer that these faults also developed during the Late Jurassic–Early Cretaceous.

The palaeostress analysis of some of these faults during the present study revealed a NNW-SSE extension direction (Figure 8(f)). This orientation lies subparallel to the NW-SE to NNW-SSE extension direction obtained from other onshore parts of the Inner Moray Firth Basin [19, 21, 22]. Based on geochronology, the resulting structures developed (within error) during the Oxfordian to Aptian ([19, 21, 22], Figure 14).

This extension direction is also parallel to that suggested by Davies et al. [49] based on offshore fault trends and analyses of seismic reflection profiles; however, they proposed a much narrower Oxfordian to early Kimmeridgian age of faulting. During the late Kimmeridgian-Tithonian, they inferred a change to NE-SW extension to explain the development of NW-SW-trending faults in the basin. Based on the present study combined with the findings of Tamas et al. [19, 21, 22], it seems that NW-SE to NNW-SSE extension directions prevailed during much of the Oxfordian to Aptian period (Figure 14). We propose that during that time, faults with different orientations and kinematics developed due to polymodal faulting and oblique reactivation of structures in various preexisting orientations (e.g. [19, 21, 22]). Thus, the observed complexity could be result of spatially variable reactivation of preexisting faults in different orientations rather than stress rotations. The NE-SW extension direction was obtained from what we infer as Cenozoic structures. This extension

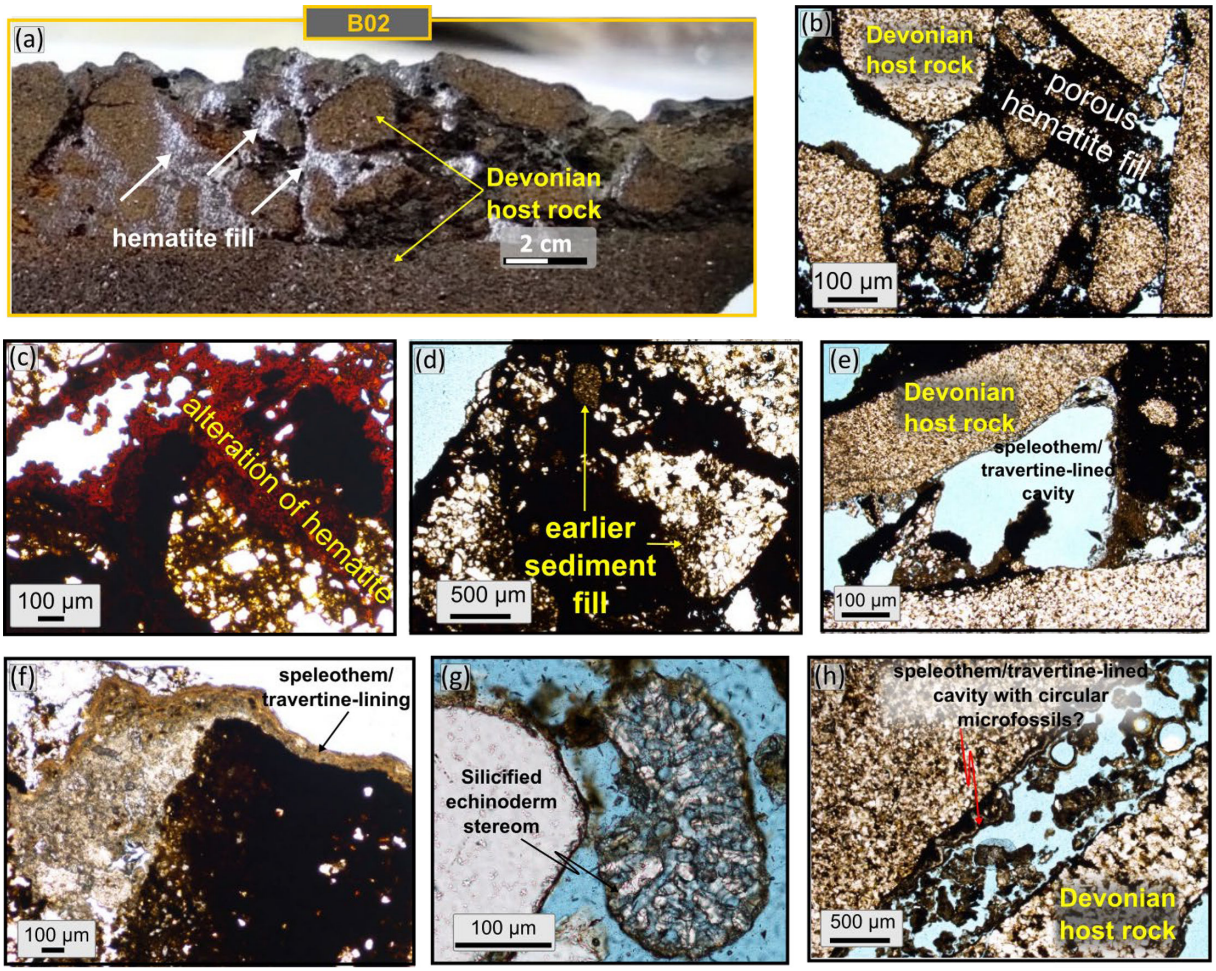

FIGURE 11: Samples and microstructures associated with calcite mineralization at Berridale 3. (a) Polished B02 hand specimen of fault breccia (b–h) representative thin section microphotographs of B01 sample showing the brecciated host rock with the pore space filled with (b) hematite and local (c) alteration of hematite to limonite (d) earlier sediment fill and (e,f) travertine/speleothem lining. (g,h) microfossils can also be observed in the cavities.

direction led to dextrally reactivated Late Jurassic–Early Cretaceous NE-SW- to ENE-WSW-trending faults and newly formed dip-slip NW-SW-trending faults onshore and offshore [20, 21].

In addition, the B03 sample which gave a c. 147 Ma age is rich in hydrocarbon inclusions (Figure 10(d)), suggesting that a period of hydrocarbon charge occurred during this episode. This also illustrates that these faults represented essential pathways for hydrocarbon migration and accumulation.

The later event characterized at Berridale by normal-dextral reactivation of the preexisting normal-sinistral ENE-WSW-trending fault is widely associated with iron-oxide staining. This event is tentatively inferred to be Cenozoic in age. This is because heavily iron oxide-stained fault planes were also observed on the southern coast at Hopeman (see [20]) where a very similar set of sinistral-normal Late Jurassic–Early Cretaceous faults was dextrally reactivated during a final phase of movement. Similarly oriented faults with this trend imaged offshore associated with the Lossiemouth Fault Zone show demonstrable Cenozoic reactivation. Cataclastically deformed calcite with deformation twins (Sample B03; Figures 7(e) and 7(f)) and fracturing with possible later sediment or iron oxide fills (Sample B01; Figure 9(i)) were also encountered in thin sections from Berridale. The heavily hematite-cemented fault breccia B02 (Figure 9(a)) shows widespread alteration to limonite (Figure 11(c)), orange-brown fibrous speleothem/travertine lining (Figure 11(f)) and marine fossils (Figure 9(g)), suggesting a complex fault history. The fault breccia could have formed earlier, related to the Jurassic - Early Cretaceous faulting, as a silicified echinoderm stereom and other marine fossil shells are found in fracture cavities. However, it seems more likely that the enrichment in iron-oxides and the hematite cement could have happened during the Cenozoic, while the alteration to limonite and the speleothem/travertine lining are most likely the results of more recent weathering in open cavities. This remains to be confirmed using geochronology.

Apart from the Late Jurassic–Early Cretaceous dates obtained calcite-mineralized fault zones, a younger age was obtained from the WS05 sample collected at Whaligoe.

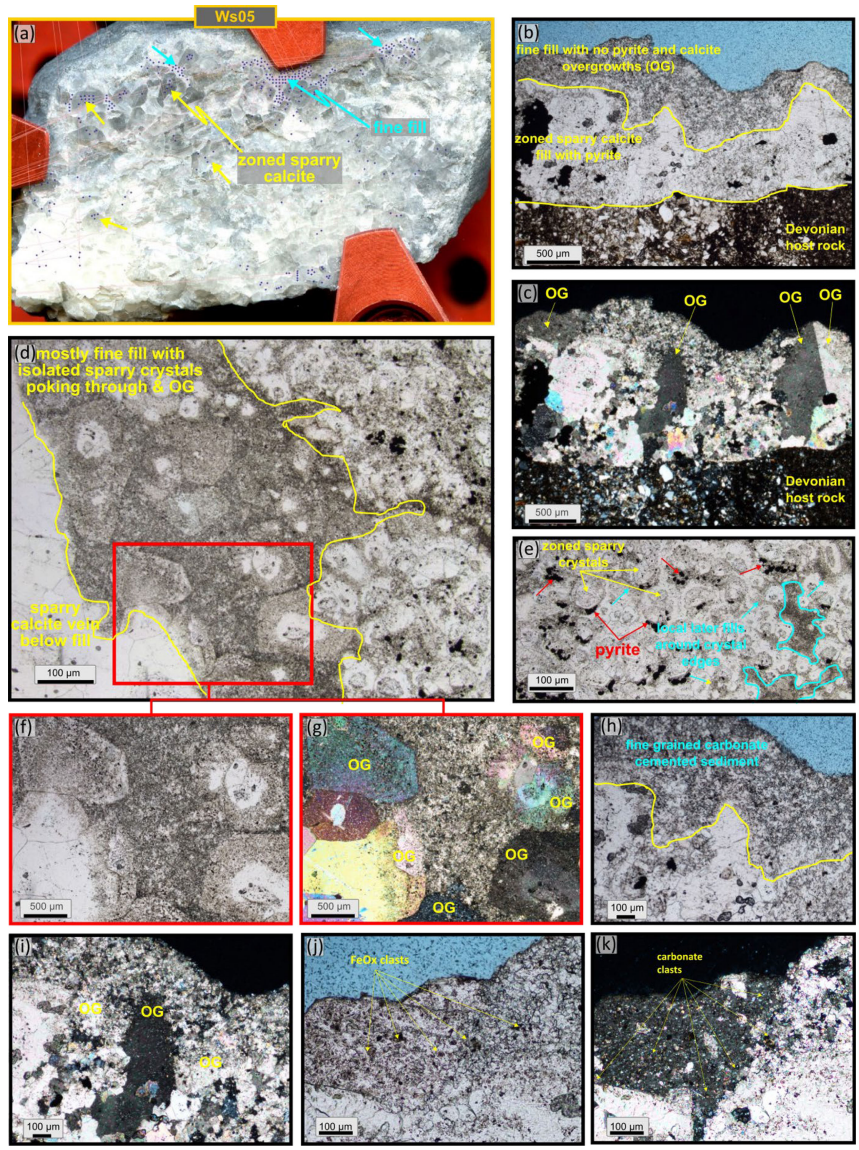

FIGURE 12: Samples and microstructures associated with calcite mineralization at Whaligoe Steps. (a) Polished thick section of mainly calcite Ws05 sample also showing the laser ablation spots (blue dots). (b–k) representative thin section microphotographs of Ws05 sample. (b) In plane polarized light, (c) crossed polarized light and the enlarged (h–k) are cut normal to vein and show an earlier sparry zoned calcite with local pyrite crystals, and a later "dusty" inclusion-rich, fine-grained carbonate with local large calcite overgrowths (OG). (**d**–**e**)—in plane polarized light) and the enlarged (f) in plane polarized light and (g) crossed polarized light, are cut at a low angle to the vein and show how the younger fill appears to infill vuggy cavities lined by early fill sparry zoned calcite. Fine inclusions including clastic carbonate and Fe oxide are visible in (j) plane polarized light and (k) crossed polarized light.

The younger Lower Miocene age (c. 19 Ma) from WS05l sample is so far unique in the Inner Moray Firth Basin, and the style of fill (Figure 12) is more consistent with a near-surface fissure passively infilled with fine grained carbonate cemented sediment (i.e. 1 deposited from above in an open fracture; for example, similar to those described from Calabria by [53]. Thus, it is not necessarily associated with a phase of active tectonism. This finding possibly confirms that (at least) Lower Miocene sediments were deposited onto the basin margin, possibly directly onto the Devonian basement and were later removed by erosion. This would agree with Hillis et al. [54], who suggest that the Late Cretaceous-Cenozoic succession was later removed by erosion and contra Roberts et al. [55], who argued that the Late Cretaceous-Tertiary sequence did not extend much to the west of the current offshore limit.

6. SUMMARY AND CONCLUSIONS

The holistic approach of this study has proved very effective in shedding new light on the nature, age, and significance of fault-related deformation events recorded in Devonian rocks of the Orcadian Basin located on the NW margin of the younger Inner Moray Firth Basin. It also confirms

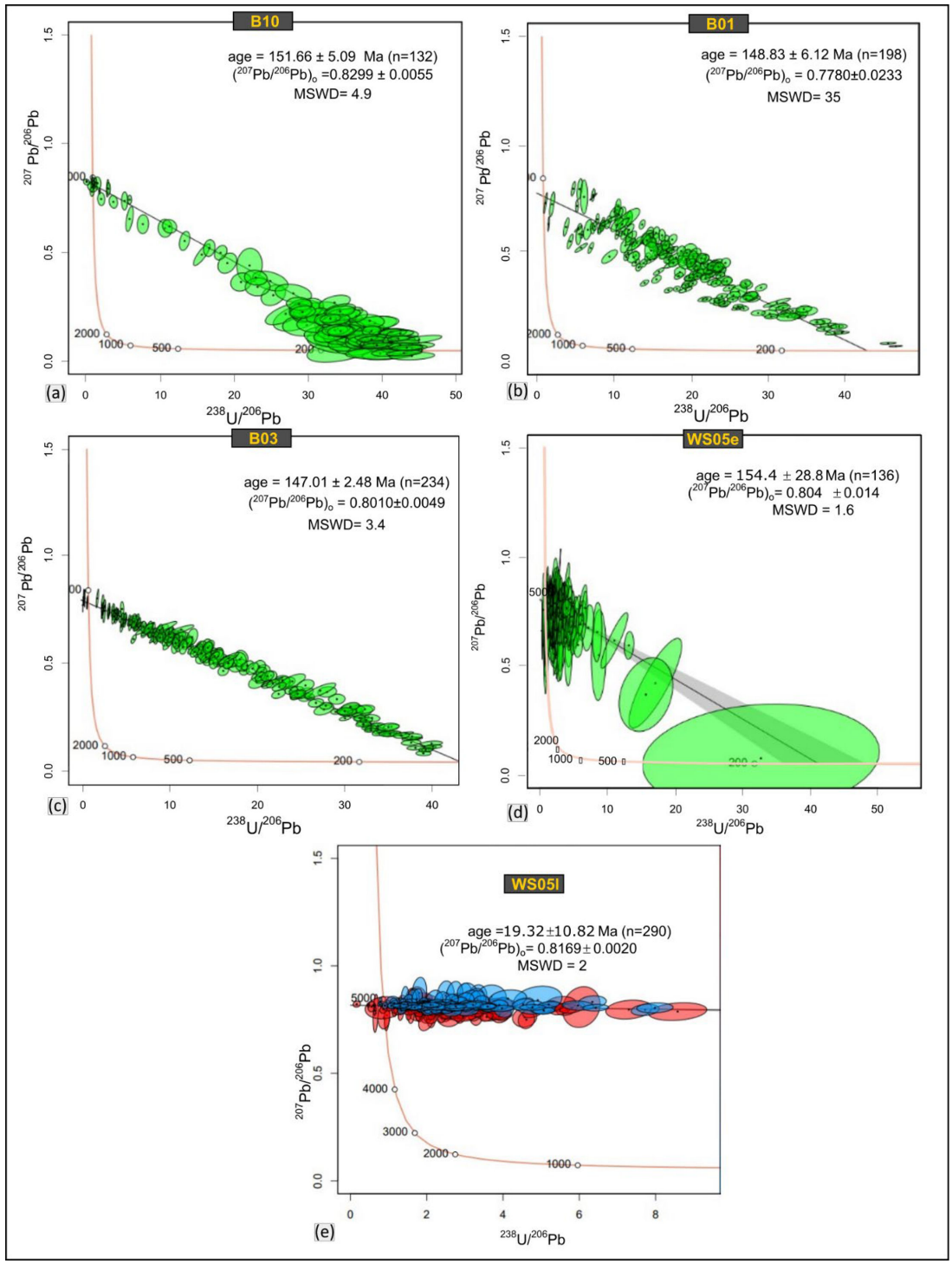

FIGURE 13: Tera–Wasserburg diagram of measured in situ calcite $^{207}Pb/^{206}Pb$ and $^{238}U/^{206}Pb$ ratios (no common lead correction) from (a) sample B01, (b) sample B03, (c) sample B10, (d) sample WS05e, and (e) WS05l. Error ellipsoids of spot analysis are plotted in green and represent 2σ uncertainties. MSWS = mean standard weighted deviation.

and enhances the known range of ages of faulting obtained around the onshore basin margins in other recent studies (e.g. [20–23]). The complex evolution of the superimposed events suggested the following deformation history, summarized in Figure 14.

6.1. Devonian

The N-S-, NNW-SSE-, and NNE-SSW-trending faults are the earliest structures observed based on cross-cutting relationships in the field. Faults with such orientations have been widely documented across the Orcadian Basin

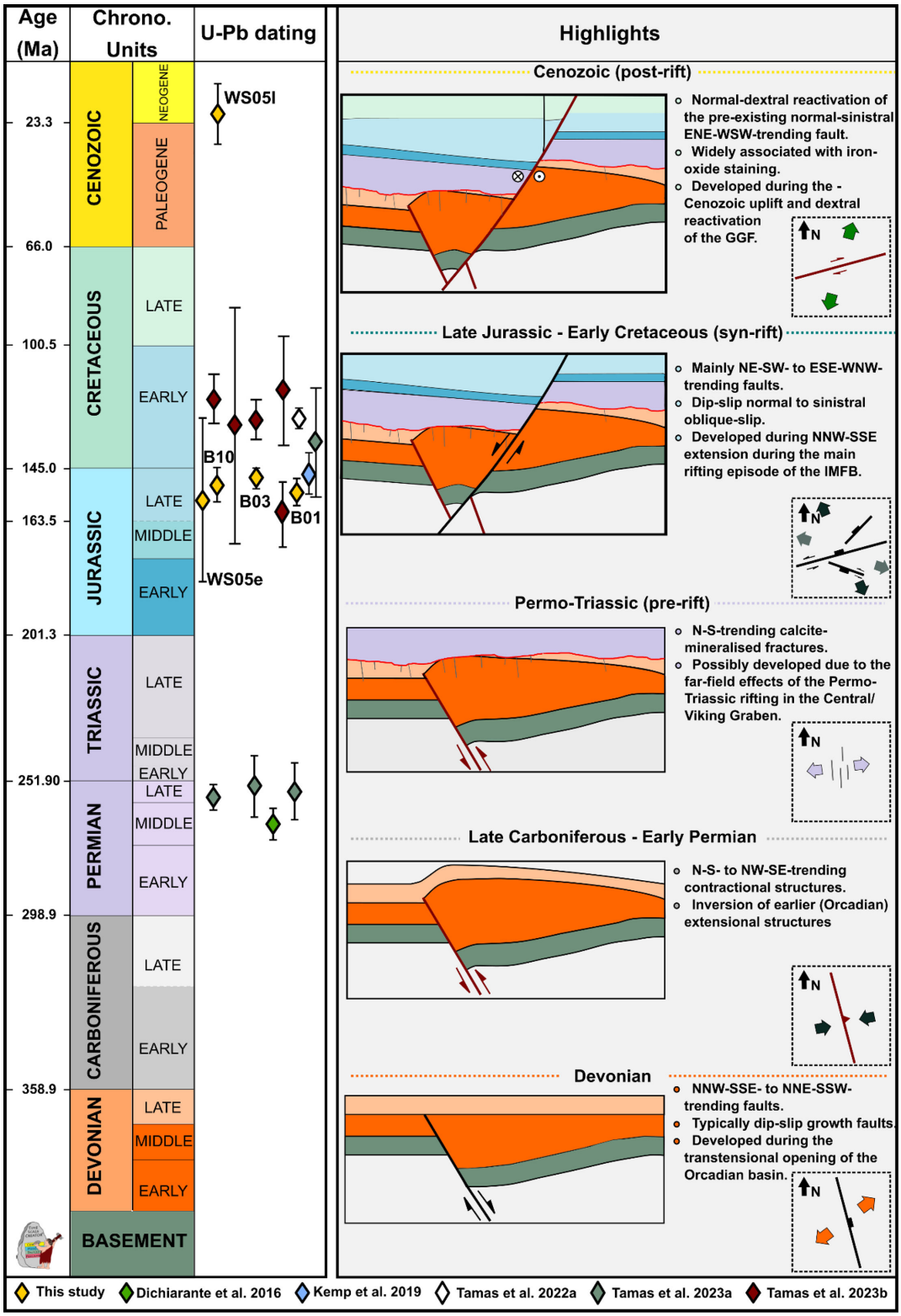

FIGURE 14: Conceptual cartoon explaining the sequential evolution of and summary of dating results against local and key regional events in the Inner Moray Firth Basin. Inset map showing the extension/compression direction and simplified map-view orientation of the most typical structures developed during that time. For all the complex fault orientation, please see the text and cited articles. Chronostratigraphic chart based on Gradstein et al.[61], generated using Time Scale Creator [62].

and commonly display growth strata in their hangingwalls. These structures are thought to be associated with sinistral shear along the Great Glen Fault Zone and associated transtensional opening of the Orcadian Basin during the

Early-Middle Devonian. There is little associated mineralization associated with these structures in the examples studied here.

6.2. Late Carboniferous–Early Permian Inversion

This episode is associated with the development of N-S-trending folds and thrusts. The compressional structures are commonly—but not exclusivel—associated with the reactivation of earlier (Devonian rift-related faults) extensional structures. These structures are interpreted as the result of a Late Carboniferous–Early Permian east-west inversion possibly related to dextral strike-slip reactivation of the nearby Great Glen Fault. Once again, in the areas studied here, there was little associated mineralization associated with these structures.

6.3. Late Permian? Minor Fracturing

N-S-trending calcite mineralized tensile veins that have the same orientation as the Late Permian age (c. 258–255 Ma) veins at Sarclet are likely the same age and could be related to the far field effects of either rifting in the Central/Viking graben of the North Sea to the east and/or to the WNW-ESE opening of the West Orkney Basin located to the north.

6.4. Late Jurassic–Early Cretaceous Rifting

Typically characterized by dip-slip to normal-sinistral oblique E-W- to NE-SW-trending faults. Some of these faults show evidence of two episodes of movement. A normal sinistral oblique-slip event, widely associated with calcite mineralization, and a later normal-dextral oblique-slip event associated with iron oxide mineralization.

As revealed by the geochronology, the calcite mineralization associated with those ENE-WSW-trending structures is Late Jurassic–Early Cretaceous (c. 154 to c. 147 Ma). This correlates well with other dates obtained from the Inner Moray Firth Basin (Figure 14). This falls within the main syn-rift episode, which led to the regional-scale opening of the basin.

6.5. Cenozoic

This faulting episode was not confirmed by calcite dating, however dextrally reactivated syn-rift faults at Berridale which are associated with iron oxide mineralization. These are similar to faults observed onshore and offshore close to the south coast of the Inner Moray Firth Basin and also to strike-slip faults observed at Sarclet.

The younger Burdigalian age (c. 19 Ma) from the later carbonate fill at Whaligoe is so far unique in the IMFB, and the style of fill is more consistent with a near-surface fissure filled with carbonate cemented sediment. It is not necessarily associated with a phase of active tectonism, but it does suggest that later Mesozoic and Cenozoic sediments did once extend northwestward onto the margins of the Inner Moray Firth Basin.

The structural-microstructural-geochronological approach adopted here can be used to characterize deformation events in other rift or superimposed rift basins worldwide. Our findings further illustrate that preexisting faults commonly localize deformation and control basin- to subbasin-scale architectures. In many cases, these structures are obliquely oriented relative to the regional extension vector and so reactivate as transtensional (e.g. normal-oblique) features with a significant component of strike-slip in addition to dip-slip. This leads to greater structural complexity because these structures may develop in addition to "new" optimally oriented rift faults. These aspects are likely critical to any subsurface investigation (e.g. for geothermal, hydrocarbon resources, or CO_2 storage) as they will create significant structural complexity and heterogeneity in potential subsurface reservoirs.

Data Availability

All of the data supporting the conclusions of the study are available in the article and its supplementary material. Additional formats or high resolution models can be requested from the corresponding author.

Conflicts of Interest

The author(s) declare(s) that there is no conflict of interest regarding the publication of this article.

Funding Statement

Based on the PhD thesis of AT undertaken as part of the Natural Environment Research Council (NERC) Centre for Doctoral Training (CDT) in Oil and Gas (NEM00578X/1) and was funded by Durham University and British Geological Survey whose support is gratefully acknowledged.

Acknowledgments

Many thanks to Nick Roberts who over the years provided valuable insights which improved geochronology data analysis. Ian Chaplin and Sophie Edwards are thanked for the thin-section preparation. We would also like to thank our anonymous reviewer and associate editor, Steve Banham, for all the useful comments that led to an improved paper.

Supplementary Materials

This article includes the following supplementary material:
Appendix A - Geochronology data;
Sketchfab links to the 3D models of Berridale and Whaligoe:
Berridale: https://skfb.ly/oXETI (last accessed 29 Iune 2024)
Whaligoe: https://skfb.ly/6S7sr (last accessed 29 Iune 2024)

REFERENCES

[1] C. A. J. Wibberley and Z. K. Shipton, "Fault zones: A complex issue", *Journal of Structural Geology*, vol. 32, no. 11, pp. 1554–1556, 2010.

[2] E. Salomon, A. Rotevatn, T. B. Kristensen, et al., "Fault-controlled fluid circulation and diagenesis along basin-bounding fault systems in rifts – Insights from the East Greenland rift system", *Solid Earth*, vol. 11, no. 6, pp. 1987–2013, 2020.

[3] R. P. Worthington and J. J. Walsh, "Timing, growth and structure of a reactivated basin-bounding fault", *Geological Society, London, Special Publications*, vol. 439, no. 1, pp. 511–531, 2017.

[4] A. M. Dichiarante, K. J. W. McCaffrey, R. E. Holdsworth, T. I. Bjørnarå, and E. D. Dempsey, "Fracture attribute scaling and connectivity in the Devonian Orcadian Basin with implications for geologically equivalent sub-surface fractured reservoirs", *Solid Earth*, vol. 11, no. 6, pp. 2221–2244, 2020.

[5] A. M. Dichiarante, R. E. Holdsworth, E. D. Dempsey, K. J. W. McCaffrey, and T. A. G. Utley, "Outcrop-scale manifestations of reactivation during multiple superimposed rifting and basin inversion events: The devonian Orcadian Basin, Northern Scotland", *Journal of the Geological Society*, vol. 178, no. 1, pp. jgs2020–089, 2021.

[6] J. P. Lovecchio, S. Rohais, P. Joseph, et al, "Multistage rifting evolution of the Colorado Basin (offshore Argentina): Evidence for extensional settings prior to the South Atlantic opening", *Terra Nova*, vol. 30, no. 5, pp. 359–368, 2018.

[7] D. Macgregor, "History of the development of the East African Rift system: A series of interpreted maps through time", *Journal of African Earth Sciences*, vol. 101, pp. 232–252, 2015.

[8] T. Ragon, A. Nutz, M. Schuster, J. Ghienne, G. Ruffet, and J. Rubino, "Evolution of the Northern Turkana depression (East African Rift system, Kenya) during the cenozoic rifting: New insights from the Ekitale Basin (28-25.5 ma)", *Geological Journal*, vol. 54, no. 6, pp. 3468–3488, 2019.

[9] M. Fournier, N. Bellahsen, O. Fabbri, and Y. Gunnell, Oblique rifting and segmentation of the NE Gulf of Aden passive margin: Oblique rifting and segmentation, *Geochemistry, Geophysics, Geosystems*, vol. 5, p. 11, 2004.

[10] J. A. Hansen, S. G. Bergh, and T. Henningsen, "Mesozoic rifting and basin evolution on the Lofoten and Vesterålen margin, North-Norway; Time constraints and regional implications", Norwegian Journal of Geology, vol. 91, pp. 203–228, 2012.

[11] G. A. Henstra, T. Berg Kristensen, A. Rotevatn, and R. L. Gawthorpe, "How do pre-existing normal faults influence rift geometry? A comparison of adjacent basins with contrasting underlying structure on the Lofoten margin, Norway", *Basin Research*, vol. 31, no. 6, pp. 1083–1097, 2019.

[12] M. Tomasso, J. R. Underhill, R. A. Hodgkinson, and M. J. Young, "Structural styles and depositional architecture in the triassic of the Ninian and Alwyn North fields: Implications for basin development and prospectivity in the Northern North sea", *Marine and Petroleum Geology*, vol. 25, no. 7, pp. 588–605, 2008.

[13] R. W. Wilson, R. E. Holdsworth, L. E. Wild, et al, "Basement-influenced rifting and basin development: A reappraisal of post-caledonian faulting patterns from the North coast transfer zone, Scotland", *Geological Society, London, Special Publications*, vol. 335, no. 1, pp. 795–826, 2010.

[14] A. M. Dichiarante, R. E. Holdsworth, E. D. Dempsey, et al, "New structural and re–os geochronological evidence constraining the age of faulting and associated mineralization in the Devonian Orcadian basin, Scotland", *Journal of the Geological Society*, vol. 173, no. 3, pp. 457–473, 2016.

[15] N. M. W. Roberts, K. Drost, M. S. A. Horstwood, et al, "Laser ablation inductively coupled plasma mass spectrometry (LA-ICP-MS) U–pb carbonate geochronology: Strategies, progress, and limitations", *Geochronology*, vol. 2, no. 1, pp. 33–61, 2020.

[16] J. R. Underhill, "Implications of mesozoic—recent basin development in the Western Inner Moray Firth, UK", *Marine and Petroleum Geology*, vol. 8, no. 3, pp. 359–369, 1991.

[17] G. S. Johnstone and W. Mykura, "British regional geology. The Northern Highlands of Scotland", in *British Geological Survey*, 1989.

[18] P. F. Friend, B. P. J. Williams, M. Ford, and E. A. Williams, "Kinematics and dynamics of old red Sandstone Basins", *Geological Society, London, Special Publications*, vol. 180, no. 1, pp. 29–60, 2000.

[19] A. Tamas, R. E. Holdsworth, J. R. Underhill, et al, "New onshore insights into the role of structural inheritance during mesozoic opening of the Inner Moray Firth Basin, Scotland", *Journal of the Geological Society*, vol. 179, no. 2, pp. jgs2021–066, 2022.

[20] A. Tamas, R. E. Holdsworth, J. R. Underhill, et al, "Correlating deformation events onshore and offshore in superimposed rift basins: The lossiemouth fault zone, Inner Moray Firth Basin, Scotland", *Basin Research*, vol. 34, no. 4, pp. 1314–1340, 2022.

[21] A. Tamas, R. E. Holdsworth, D. M. Tamas, et al, "Using UAV-based photogrammetry coupled with *in situ* fieldwork and U-pb geochronology to decipher multi-phase deformation processes: A case study from sarclet, Inner Moray Firth Basin, UK", *Remote Sensing*, vol. 15, no. 3, p. 695, 2023.

[22] A. Tamas, R. E. Holdsworth, D. M. Tamas, et al, "Older than you think: Using U–pb calcite geochronology to better constrain basin-bounding fault reactivation, Inner Moray Firth Basin, Western North sea", *Journal of the Geological Society*, vol. 180, no. 5, pp. jgs2022–166, 2023.

[23] N. M. W. Roberts and R. E. Holdsworth, "Timescales of faulting through calcite geochronology: A review", *Journal of Structural Geology*, vol. 158, p. 104578, 2022.

[24] D. A. Rogers, J. E. A. Marshall, and T. R. Astin, "Short paper: Devonian and later movements on the Great Glen Fault system, Scotland", *Journal of the Geological Society*, vol. 146, no. 3, pp. 369–372, 1989.

[25] J. E. A. Marshall and A. J. Hewett, "Petroleum geology of the 612 central and Northern North sea, geological society of London", in *The Millenium Atlas*, D. Evans, C. Graham, A. Armour, and P. Bathrust, Eds., pp. 105–128, 2003.

[26] M. Seranne, "Devonian extensional tectonics versus carboniferous inversion in the Northern Orcadian Basin", *Journal of the Geological Society*, vol. 149, no. 1, pp. 27–37, 1992.

[27] W. I. Duncan and N. W. K. Buxton, "New evidence for evaporitic middle devonian lacustrine sediments with hydrocarbon source potential on the East shetland platform,

North sea", *Journal of the Geological Society*, vol. 152, no. 2, pp. 251–258, 1995.

[28] N. Woodcock and R. Strachan, eds., *Geological History of Britain and Ireland*. 1st ed, Wiley, 2012.

[29] H. Fossen, "Extensional tectonics in the North Atlantic caledonides: A regional view", *Geological Society, London, Special Publications*, vol. 335, no. 1, pp. 767–793, 2010.

[30] J. F. Dewey and R. A. Strachan, "Changing silurian–devonian relative plate motion in the caledonides: Sinistral transpression to sinistral transtension", *Journal of the Geological Society*, vol. 160, no. 2, pp. 219–229, 2003.

[31] L. M. Watts, R. E. Holdsworth, J. A. Sleight, R. A. Strachan, and S. A. F. Smith, "The movement history and fault rock evolution of a reactivated crustal-scale strike-slip fault: The walls boundary fault zone, Shetland", *Journal of the Geological Society*, vol. 164, no. 5, pp. 1037–1058, 2007.

[32] M. A. Enfield and M. P. Coward, "The structure of the West Orkney Basin, Northern Scotland", *Journal of the Geological Society*, vol. 144, no. 6, pp. 871–884, 1987.

[33] J. Parnell, P. Carey, and B. Monson, "Timing and temperature of decollement on hydrocarbon source rock beds in cyclic lacustrine successions", *Palaeogeography, Palaeoclimatology, Palaeoecology*, vol. 140, no. 1–4, pp. 121–134, 1998.

[34] T. B. Armitage, L. M. Watts, R. E. Holdsworth, and R. A. Strachan, "Late carboniferous dextral transpressional reactivation of the crustal-scale walls boundary fault, Shetland: The role of pre-existing structures and lithological heterogeneities", *Journal of the Geological Society*, vol. 178, no. 1, pp. jgs2020–078, 2021.

[35] T. A. G. Utley, R. E. Holdsworth, R. J. Walker, et al, "An onshore-offshore interpretation of structures in the devonian rocks of the Pentland Firth, Scotland using high resolution bathymetry and drone-enabled field observations", *Journal of Structural Geology*, vol. 174, p. 104922, 2023.

[36] M. P. Coward, M. A. Enfield, and M. W. Fischer, "Devonian basins of Northern Scotland: Extension and inversion related to late caledonian — variscan tectonics", *Geological Society, London, Special Publications*, vol. 44, no. 1, pp. 275–308, 1989.

[37] S. J. Kemp, M. R. Gillespie, G. A. Leslie, H. Zwingmann, and S. D. G. Campbell, "Clay mineral dating of displacement on the sronlairig fault: Implications for mesozoic and cenozoic tectonic evolution in Northern Scotland", *Clay Minerals*, vol. 54, no. 2, pp. 181–196, 2019.

[38] J. R. Underhill and J. A. Brodie, "Structural geology of easter ross, Scotland: Implications for movement on the Great Glen Fault zone", *Journal of the Geological Society*, vol. 150, no. 3, pp. 515–527, 1993.

[39] E. Le Breton, P. R. Cobbold, and A. Zanella, "Cenozoic reactivation of the Great Glen Fault, Scotland: Additional evidence and possible causes", *Journal of the Geological Society*, vol. 170, no. 3, pp. 403–415, 2013.

[40] N. Cardozo and R. W. Allmendinger, "Spherical projections with osxstereonet", *Computers & Geosciences*, vol. 51, pp. 193–205, 2013.

[41] J. Angelier, "Inversion of field data in fault tectonics to obtain the regional stress-III. A new rapid direct inversion method by analytical means", *Geophysical Journal International*, vol. 103, no. 2, pp. 363–376, 1990.

[42] Á. Sasvári and A. Baharev, "SG2PS (structural geology to postscript converter) – A graphical solution for brittle structural data evaluation and paleostress calculation", *Computers & Geosciences*, vol. 66, pp. 81–93, 2014.

[43] D. M. Tămaş, A. Tămaş, J. Barabasch, et al, "Low-Angle shear within the exposed Mânzălești diapir, Romania: Salt decapitation in the eastern Carpathians fold-and-thrust belt", *Tectonics*, vol. 40, no. 6, 2021.

[44] R. E. Holdsworth, R. Trice, K. Hardman, et al, "The nature and age of basement host rocks and fissure fills in the Lancaster field fractured reservoir, West of Shetland", *Journal of the Geological Society*, vol. 177, no. 5, pp. 1057–1073, 2020.

[45] P. Vermeesch, "IsoplotR: A free and open toolbox for geochronology", *Geoscience Frontiers*, vol. 9, no. 5, pp. 1479–1493, 2018.

[46] "BGS'geological map, latheron,'" in *Scotland Sheet*. Vol. 50, 1985.

[47] R. N. Donovan, "Devonian lacustrine limestones at the margin of the Orcadian Basin, Scotland", *Journal of the Geological Society*, vol. 131, no. 5, pp. 489–510, 1975.

[48] R. N. Donovan, R. J. Foster, and T. S. Westoll, "8.—A stratigraphical revision of the old red sandstone of North-Eastern caithness", *Transactions of the Royal Society of Edinburgh*, vol. 69, no. 8, pp. 167–201, 1974.

[49] R. J. Davies, J. D. Turner, and J. R. Underhill, "Sequential dip-slip fault movement during rifting: A new model for the evolution of the jurassic trilete North sea rift system", *Petroleum Geoscience*, vol. 7, no. 4, pp. 371–388, 2001.

[50] D. Healy, R. R. Jones, and R. E. Holdsworth, "Three-dimensional brittle shear fracturing by tensile crack interaction", *Nature*, vol. 439, no. 7072, pp. 64–67, 2006.

[51] D. Healy, T. G. Blenkinsop, N. E. Timms, P. G. Meredith, T. M. Mitchell, and M. L. Cooke, "Polymodal faulting: Time for a new angle on shear failure", *Journal of Structural Geology*, vol. 80, pp. 57–71, 2015.

[52] K. Thomson and J. R. Underhill, "Controls on the development and evolution of structural styles in the Inner Moray Firth Basin", *Geological Society, London, Petroleum Geology Conference Series*, vol. 4, no. 1, pp. 1167–1178, 1993.

[53] K. Hardman, R. E. Holdsworth, G. Palladino, G. Prosser, Z. Killingback, and K. J. W. McCaffrey, "Geology and evolution of fissure systems in fractured basement rocks, Calabria, Southern Italy: Implications for sub-unconformity reservoirs and aquifers", *Journal of the Geological Society*, vol. 180, no. 3, pp. jgs2022–085, 2023.

[54] R. R. Hillis, K. Thomson, and J. R. Underhill, "Quantification of tertiary erosion in the Inner Moray Firth using sonic velocity data from the chalk and the kimmeridge clay", *Marine and Petroleum Geology*, vol. 11, no. 3, pp. 283–293, 1994.

[55] A. M. Roberts, M. E. Badley, J. D. Price, and I. W. Huck, "The structural history of a transtensional basin: Inner Moray Firth, NE Scotland", *Journal of the Geological Society*, vol. 147, no. 1, pp. 87–103, 1990.

[56] P. J. Goldsmith, G. Hudson, and P. Veen, "Petroleum geology of the 612 Central and Northern North sea, geological society of London", in *The Millenium Atlas*, D. Evans, C. Graham, A. Armour, and P. Bathrust, Eds., pp. 105–128, 2003.

[57] P. C. Bird, J. A. Cartwright, and T. L. Davies, "Basement reactivation in the development of rift basins: An example of reactivated caledonide structures in the West Orkney Basin", *Journal of the Geological Society*, vol. 172, no. 1, pp. 77–85, 2015.

[58] N. H. Trewin and A. R. Hurst, eds., *Excursion Guide to the Geology of East Sutherland and Caithness*. 2. ed, Dunedin Academic Press, Edinburgh, 2009.

[59] T. P. Fletcher, C. A. Auton, A. J. Highton, J. W. Merritt, S. Robertson, K. E. Rollin, et al, *Geology of Fortrose and Eastern Inverness District: Memoir for 1:50000 Geological Sheet 84W*, HMSO, Scotland, 1996.

[60] N. H. Trewin and M. F. Thirlwall, *Old Red Sandstone*. 4th ed, The Geology of Scotland Geological Society, Londonp, in, 2002.

[61] F. M. Gradstein, J. G. Ogg, M. Schmitz, and G. OggGeologic time scale 2020, Elsevier, 2020.

[62] T. S. CreatorTime Scale Creator Version 8.1. Geologic TimeScale Foundation, 2021.